1 **Seasonal cycles of biogeochemical fluxes in the Scotia Sea, Southern Ocean: A stable isotope**
2 **approach**

3

4 Anna Belcher[1], Sian F. Henley[2], Katharine Hendry[1,3], Marianne Wootton[4], Lisa Friberg[3], Ursula
5 Dallman[2], Tong Wang[3], Christopher Coath[3], Clara Manno[1]

6 [1] British Antarctic Survey, Cambridge, CB3 0ET, UK

7 [2] School of Geosciences, University of Edinburgh, Edinburgh EH9 3FE, UK

8 [3] University of Bristol, Bristol, BS8 1RJ, UK

9 [4] Marine Biological Association, Plymouth, PL1 2PB, UK

10

11 Correspondence to: Anna Belcher (annbel@bas.ac.uk) and Clara Manno (clanno@bas.ac.uk)

12

13 **Abstract**

14 The biological carbon pump is responsible for much of the decadal variability in the ocean carbon
15 dioxide (CO_2) sink, driving the transfer of carbon from the atmosphere to the deep ocean. A
16 mechanistic understanding of the ecological drivers of particulate organic carbon (POC) flux is key to
17 both the assessment of the magnitude of the ocean CO_2 sink, as well as for accurate predictions as to
18 how this will change with changing climate. This is particularly important in the Southern Ocean, a
19 key region for the uptake of CO_2 and the supply of nutrients to the global thermocline. In this study
20 we examine sediment trap derived particle fluxes and stable isotope signatures of carbon (C),
21 nitrogen (N) and biogenic silica (BSi) at a study site in the biologically productive waters of the
22 northern Scotia Sea in the Southern Ocean. Both deep (2000 m) and shallow (400 m) sediment traps
23 exhibited two main peaks in POC, particulate nitrogen and BSi flux, one in austral spring and one in
24 summer, reflecting periods of high surface productivity. Particulate fluxes and isotopic compositions
25 were similar in both deep and shallow sediment traps, highlighting that most remineralisation
26 occurred in the upper 400 m of the water column. Differences in the seasonal cycles of isotopic
27 compositions of C, N and Si provide insights into the degree of coupling of these key nutrients. We
28 measured increasing isotopic enrichment of POC and BSi in spring, consistent with fractionation
29 during biological uptake. Since we observed isotopically light particulate material in the traps in
30 summer, we suggest physically-mediated replenishment of lighter isotopes of key nutrients from
31 depth, enabling full expression of the isotopic fractionation associated with biological uptake. The
32 change in the nutrient and remineralisation regimes, indicated by the different isotopic
33 compositions baselines of the spring and summer productive periods, suggests to a change in the
34 source region of material reaching the traps, and associated shifts in phytoplankton community
35 structure. This, combined with the occurrence of advective inputs at certain times of the year,
36 highlights the need to make synchronous measurements of physical processes to improve our ability
37 to be able to better track changes in the source regions of sinking particulate material. We also
38 highlight the need to conduct particle-specific (e.g. faecal pellet, phytoplankton detritus,
39 zooplankton moults) isotopic analysis to improve the use of this tool in assessing particle

40 composition of sinking ~~particulate~~ the material and develop our understanding of the drivers of

41 biogeochemical fluxes.

42

1. Introduction

44 The transfer of carbon from the atmosphere to the deep ocean via the biological carbon pump (~~BCP,~~

45 Volk and Hoffert, 1985) is important for the sequestration of carbon, and combined with ocean

46 circulation is a main driver of decadal variability of the ocean carbon dioxide (CO_2) sink (DeVries,

47 2022). Mechanistic understanding of the processes controlling the magnitude and efficiency of the

48 biological carbon pump~~BCP~~ is therefore key to assessment and prediction of the ocean's role as a

49 CO_2 sink and requires robust characterisation of the composition of the sinking particles transferring

50 particulate organic carbon (POC) to the deep ocean. The composition of particles affects the sinking

51 rate, lability and thus degree of remineralisation as they~~it~~ sink~~s~~ through the water column (e.g. Ploug

52 et al., 2008; Giering et al., 2020).

53 Sediment traps enable visual assessment of sinking particles, and have been deployed in numerous

54 locations throughout the world's oceans to both quantify biogeochemical fluxes and characterise the

55 nature of sinking material (for example data compilation of Atlantic Ocean sediment traps; Torres

56 Valdés et al., 2014). Sediment traps can be susceptible to collection biases depending on the depth

57 of deployment, trap design, hydrodynamic conditions and properties of sinking particles (Buesseler

58 et al., 2007). Moored sediment traps can underestimate the actual flux ~~collect~~ at depths shallower

59 than ~1500 m by collecting only a portion of the sinking material, though biases vary greatly

60 between sites (Buesseler et al., 2007). Numerous studies have recorded the dominance of particular

61 organisms or types of detrital material in trap material, highlighting the importance of ecosystem

62 community structure on the magnitude and efficiency of the biological carbon pump~~BCP~~. For

63 example, faecal pellets, diatoms, diatom resting spores and acantharia have been observed as

64 significant contributors to particle fluxes (González et al., 2009; Belcher et al., 2018, 2017; Manno et

65 al., 2015; Gleiber et al., 2012; Rembauville et al., 2015; Roca-Marti et al., 2017). Such visual

66 assessment of trap material is typically very time consuming. Additionally, fragile material, such as

67 salp faecal pellets (Iversen et al., 2017; Pauli et al., 2021) may break up in the sample manipulation

68 processes, making them hard to account for visually. Biogeochemical methods such as the use of

69 stable isotopes may offer additional insight into the drivers of POC fluxes (e.g. Henley et al., 2012).

70 Marine phytoplankton take up aqueous CO_2 ($[CO_{2(aq)}]$) during photosynthesis, converting it to organic

71 carbon. During this process, the lighter isotope (^{12}C) is preferentially assimilated, which enriches the

72 residual aqueous pool in the heavier isotope (^{13}C). The stable isotopic composition of the POC

73 ($\delta^{13}C_{POC}$) of the marine phytoplankton is therefore lower than that of the carbon source. Over large

74 scales, the $\delta^{13}C$ of marine phytoplankton has been found to be inversely correlated with $[CO_{2(aq)}]$ in

75 surface waters (Rau et al., 1991). However, numerous other factors have been identified as

76 impacting the $\delta^{13}C_{POC}$ of surface waters and marine plankton. Phytoplankton growth rates, cell

77 geometry and non-diffusive uptake of carbon via carbon concentration mechanisms have all been

78 highlighted as impacting the $\delta^{13}C_{POC}$ of marine plankton and thus surface waters (Popp et al., 1999,

79 1998; Bidigare et al., 1999; Trull and Armand, 2001; Tuerena et al., 2019). This decoupling of the

80 relationship between $\delta^{13}C_{POC}$ and $[CO_{2(aq)}]$ presents ~~complications~~ challenges for palaeoceanographic

81 studies, but ~~presents~~ also the possibility of using the $\delta^{13}C_{POC}$ of marine samples to infer information
82 about community composition.

83 During photosynthetic uptake, the balance between supply and demand of carbon impacts $\delta^{13}C_{POC}$,
84 regulated by the transport into the internal cell and fixation to organic carbon (Popp et al., 1999;
85 Trull and Armand, 2001). A greater isotopic fractionation occurs in smaller phytoplankton cells,
86 enabled by the higher cell surface area to volume (SA:V) ratios and increased amount of $[CO_{2(aq)}]$
87 diffusing across the cell membrane relative to the total carbon within the cell (Popp et al., 1998;
88 Tuerena et al., 2019; Hansman and Sessions, 2016). Thus, a community dominated by large, fast-
89 growing diatoms is expected to contribute to enriched $\delta^{13}C_{POC}$ values compared to a community
90 dominated by picoplankton. A study by Henley et al. (2012) in the coastal western Antarctic
91 Peninsula, attributed a large (~10 ‰) negative isotopic shift in $\delta^{13}C_{POC}$ to a near-complete biomass
92 dominance of the marine diatom *Proboscia inermis* highlighting the possible impact of shifts in
93 species composition on stable isotopes. It may therefore be possible to use stable isotopes to gain
94 information about the community composition of phytoplankton driving, for example, large spring
95 pulses in POC flux. Additionally, siliceous phytoplankton, such as diatoms, require dissolved silica
96 (silicic acid, or DSi) to build their cell walls or frustules (amorphous $SiO_2 \cdot nH_2O$, referred to here as
97 biogenic silica, BSi). During uptake of DSi, diatoms fractionate the stable isotopes of silicon (^{28}Si, ^{29}Si,
98 ^{30}Si) preferentially taking up the lighter isotopes ~~and isotopic fractionation occurs~~ during cell wall
99 (frustule) formation (De La Rocha et al., 1997). This means that BSi fluxes and ratios of light ^{28}Si to
100 heavy ^{30}Si (expressed as $\delta^{30}Si$) in sinking particulate organic matter (POM) can be informative about
101 DSi utilisation by siliceous phytoplankton. The fractionation of Si isotopes during diatom DSi
102 utilisation is approximately -1.1 ‰, although estimates of this value vary in laboratory and field
103 studies between -0.5 and -2. 5‰ (Hendry and Brzezinski, 2014). Whilst some studies have shown
104 that isotopic fractionation is independent of temperature, DSi and diatom species (e.g., De La Rocha
105 et al., 1997), one *in vitro* laboratory culture experiment revealed a potential species effect, with
106 polar species exhibiting more extreme fractionation (-2.09 ‰ for *Chaetoceros* sp. and 0.54 ‰
107 *Fragilariopsis kerguelensis*, (Sutton et al., 2013). The impact of water column dissolution on frustule
108 $\delta^{30}Si$ is poorly constrained, with experimental evidence for either a small fractionation of -0.55 ‰
109 (Demarest et al., 2009) or a negligible impact (Wetzel et al., 2014; Egan et al., 2012; Grasse et al.,
110 2021)~~(Wetzel et al., 2014; Egan et al., 2012)~~.

111 Additionally, the stable isotopes of marine nitrogen reveal information about uptake of inorganic
112 nitrogen sources by phytoplankton (Wada and Hattori, 1978), as well as trophic and food web
113 processes (Michener and Lajtha, 2008). Nitrogen has two isotopes, ^{14}N, and ^{15}N, and the ratio
114 between these heavy and light isotopes is expressed as $\delta^{15}N$. Different sources of nitrogen can alter
115 the ~~baseline~~ stable isotopic composition ~~($\delta^{15}N$)~~ of marine phytoplankton because ammonium
116 characteristically has a lower value of $\delta^{15}N$ than nitrate supplied from depth. As well as this, isotopic
117 fractionation occurs during transfer through the food -web, with a trophic enrichment of typically 2-
118 4 ‰ between successive trophic levels (Montoya, 2007; Minagawa and Wada, 1984). Excretion and
119 egestion processes can impact $\delta^{15}N$; isotopic discrimination during excretion of ammonium by
120 zooplankton and fish results in ammonium that is ^{15}N-depleted relative to the substrate catabolised
121 (Montoya, 2007). Thus, there are several interacting processes impacting the degree of fractionation
122 and subsequent isotopic ratios in particulate nitrogen (PN) and knowledge of $\delta^{15}N$ ratios may
123 provide insight into biogeochemical processes and the composition of the sinking flux.

124 In this study we examine the seasonal cycle~~,~~ of the magnitude and composition of vertical

125 biogeochemical fluxes of particulate material collected by two sediment traps deployed for almost

126 one year ~~year~~ on a deep ocean mooring located in the northern Scotia Sea in the ~~(~~Atlantic sector of

127 the Southern Ocean~~)~~. The Scotia Sea, particularly the region downstream of South Georgia is a hot

128 spot for biological productivity, supported by higher iron availability (Korb et al., 2008; Matano et al.,

129 2020). Diatoms dominate the phytoplankton assemblage, particularly in the summer months, with

130 smaller contributions of dinoflagellates (Korb et al., 2012). The large, consistent phytoplankton

131 blooms occurring in this region support high fluxes of POC to the deep ocean, with two peaks in POC

132 flux occurring during the seasonal cycle~~;~~ (first peak in austral spring, and second in late summer or

133 early autumn~~)~~ (Manno et al., 2015). Faecal pellets (up to 91 % in late spring and early summer,

134 ~~seasonally~~ (Manno et al., 2015)~~)~~, krill exuviae (up to 47 % in summer, ~~seasonally~~ (Manno et al.,

135 2020)~~)~~ and diatoms, particularly resting spores (annual contribution of 42 %, ~~annually~~ (Rembauville

136 et al., 2016)~~)~~ have been shown to make ~~a~~ large contributions to the POC fluxes in our study region.

137 Here we use $\delta^{13}C_{POC}$, $\delta^{15}N_{PN}$ and $\delta^{30}Si_{BSi}$ alongside calculated fluxes of POC, PN and BSi as tools to

138 reveal information ~~on the composition of~~ about sinking particulate organic matter and the processes

139 influencing its production and subsequent flux to depth. More in-depth understanding of the

140 composition, and thus the drivers of POC flux in this important region are key to improving estimates

141 of the current and future strength of the biological carbon pump~~BCP~~ and the ocean's role as a CO_2

142 sink.

143

144 **2. Methods**

145 *2.1. Study Area*

146 This study was conducted in the open ocean environment of the northern Scotia Sea in the Southern

147 Ocean at a long-term observatory station, P3 (Figure 1), where an oceanographic mooring is located.

148 The mooring is part of the Scotia Sea Open Ocean Observatory (SCOOBIES:

149 https://www.bas.ac.uk/project/scoobies/), a programme designed to investigate the biological and

150 biogeochemical influence of the large and persistent phytoplankton bloom to the northwest of

151 South Georgia.

152
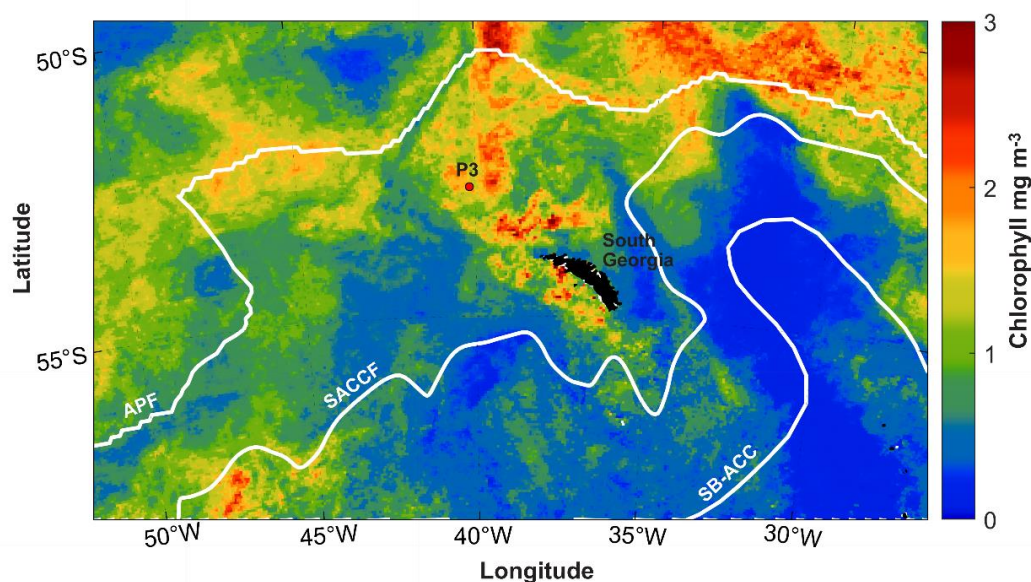
Figure 1: Location of P3 mooring site to the northwest of South Georgia. White lines indicate frontal positions of the Antarctic Polar Front (APF) (Moore et al., 1999)*, Southern ~~Atlantic~~Antarctic Circumpolar Current Front (SACCF)* (Thorpe et al., 2002) *and the Southern Boundary of the Antarctic Circumpolar Current (SB-ACC)* (Orsi et al., 1995)*. Mean chlorophyll concentration (mg m^{-3}) is shown for December 2018 from 8--day satellite chlorophyll data from the Ocean Colour CCI (version 5.0)* (Sathyendranath et al., 2021, 2019)*.*

2.2. Sediment trap deployment

Two sediment traps were deployed on the mooring array to collect sinking particles for analysis of carbon, nitrogen and biogenic silica fluxes and analysis of $\delta^{13}C_{POC}$, $\delta^{15}N_{PN}$ and $\delta^{30}Si_{BSi}$. The mooring was deployed from 25th January 2018, during research cruise JR17002 aboard the *RRS James Clark Ross,* to 1st January 2019, recovered during research cruise DY098 aboard the *RRS Discovery.* The mooring was located at –52.8036 °S~~N~~, –40.1593 °W~~E~~, to the northwest of South Georgia island in the Scotia Sea at a water depth of 3748 m. Sediment traps (McLane PARFLUX, 0.5 m^2 surface collecting area; McLane labs, Falmouth, MA, USA) were deployed at 400 and 2000 m (referred herein as shallow and deep respectively) and were each equipped with 21 sample bottles. A baffle at the top of the trap prevents large organisms from entering and each sample bottle contained a formosaline solution (filtered seawater containing 2 % v/v formalin, mixed with sodium tetraborate (BORAX; 0.025 % w/v), and 0. 5% w/v sodium chloride) to prevent mixing with the overlying water column and stop biological degradation. Previous studies have reported the effects of formalin on $\delta^{13}C_{POC}$ and $\delta^{15}N_{PN}$ to be small (±1 ‰ and ±1.5 ‰ respectively, (Mincks et al., 2008 and references therein~~s.within)~~. This ~~which~~ equates to 13 %~~.3~~ and 16~~5.8~~ % of the maximum range measured in our study~~)~~ ~~(Mincks et al., 2008 and refs. within)~~, which is~~are~~ small compared to the isotopic shifts we observed. Yet we stress that all $\delta^{13}C_{POC}$ and $\delta^{15}N_{PN}$ ~~given~~ values given here are associated with this uncertainty. The sediment trap sample carrousel was programmed to rotate every 7-31 days depending on the season; shorter periods to coincide with austral summer and longer periods during austral winter (Table S1). TM Seaguard current meters were deployed ~50 m above the shallow sediment trap and 50 m below the ~~/below the shallow/~~deep sediment trap~~s respectively~~, set at a measurement interval of 2 hours.

2.3. Trap sample processing

Each sample bottle from the sediment trap was processed on return to the laboratory. The supernatant was carefully removed using a syringe and swimmers (zooplankton that are believed to have entered the trap actively whilst alive) were removed. Swimmers were removed by hand under a dissecting microscope and were not included in flux calculations. The material from ~~E~~each sediment trap sample bottle was split into a number of smaller aliquots for subsequent analysis using a McLane rotary splitter.

2.3.1. Organic carbon and nitrogen

For each sediment trap ~~sample~~ bottle (from both deep and shallow traps~~)~~, two or three splits were taken and each analysed for POC and PN mass and $\delta^{13}C_{POC}$ and $\delta^{15}N_{PN}$. Once split, the material was filtered onto pre-combusted (450 °C, 16h) 25 mm glass fibre filters (GF/F; nominal pore size 0.7 µm)

194 and rinsed with milli-Q water. Samples were air dried, ~~before~~ fum~~ed~~ing for 24 h with 37_% HCl in a

195 desiccator, before finally oven-drying at 50 °C for 24 h. Filters and filter blanks were placed in sterile

196 tin capsules and POC and PN measured on a CE Instruments NA2500 Elemental analyser, calibrated

197 using an acetanilide calibration standard with a known %C and %N of 71.09_% and 10.36_%

198 respectively. Standards were interspersed regularly between samples to measure and correct for

199 drift. Analytical precision was better than 1.0_% for POC and 1.1_% for PN. The POC flux (F, $mg\ C\ m^{-2}$

200 d^{-1}) for each sample was calculated using the following equation:

201 $$F~~(mg\ C\ m^{-2}d^{-1})~~ = m/(A \times d) \tag{1}$$

202 Here m is the mass of POC in the sample bottle (mg), d is the number of days that the sample bottle

203 was open (7–31 days) and A is the surface area of the sediment trap opening (0.5 m^2). The same

204 calculation was carried out for PN.

205 ~~An additional two splits were taken from each sample bottle for analysis of both~~ $\delta^{13}C_{POC}$ and $\delta^{15}N_{PN}$.

206 ~~These samples were processed as above for POC and PN but~~ were analysed on a Thermo Finnigan

207 Delta-Plus Advantage isotope ratio mass spectrometer that was in line with the elemental analyser.

208 All $\delta^{13}C_{POC}$ and $\delta^{15}N_{PN}$ data are presented in the~~as~~ delta per mille (‰) notation~~enrichment~~ relative to

209 the appropriate international ~~a~~standard, according to equation 2.

210 $$\delta X(‰) = 10^3 \left(R_{sample}/R_{standard} - 1 \right) \tag{2}$$

211 ~~where~~ R denotes the $^{13}C/^{12}C$ ratio for carbon or the $^{15}N/^{14}N$ ratio for nitrogen. R_{sample} refers to the

212 relevant ratio in the sample. $R_{standard}$ refers to the ratios in the international standard~~s~~ Vienna Pee

213 Dee belemnite (V-PDB ~~used as reference material~~ for $\delta^{13}C$ and atmospheric nitrogen (AIR) for $\delta^{15}N$

214 ~~which is Vienna Pee Dee belemnite (V-PDB) and atmospheric nitrogen (AIR) respectively~~, both of

215 which ~~we~~are calibrated against the PACS-2 marine sediment reference material ~~international~~

216 ~~standard~~. Multiple repeats of analytical standards gives a reproducibility of 0.2_‰ for C and N, which

217 is significantly smaller than the uncertainty associated ~~possible effects~~with ~~of~~ organic carbon in the

218 formalin preservat~~ive~~ion (±1_‰ and ±1.5_‰ for C and N respectively,~~)~~ (Mincks et al., 2008 and

219 r~~ef~~eferences therein~~fs. within~~).

220

221 *2.3.2.Biogenic silica*

222 Two splits were taken f~~o~~rom~~r~~ each ~~sediment trap~~ sample bottle~~ample~~ (from both deep and shallow

223 sediment traps~~)~~ for analysis of biogenic silica and silicon isotopes. Split material was filtered onto 25

224 mm, 0.4 µm, polycarbonate filters and rinsed with Milli-Q water before drying at 50 °C for 24h.

225 Material on the filters was solubilised via an alkaline extraction method (Hatton et al., 2019) carried

226 out at the Bristol Isotope Group (BIG) laboratory. Sample material was digested in Teflon tubes with

227 0.2M NaOH at 100 °C for 40 minutes. This was followed by neutralisation with 6M HCl. Biogenic silica

228 (SiO$_2$, termed BSi) concentrations were measured chlorometrically by molybdate blue

229 spectrophotometry (Heteropoly Blue Method) (Strickland and Parsons, 1972) using a Hach DR3900

230 spectrophotometer set at a wavelength of 815 nm. Supernatants were stored for 7-11 months

231 before column chemistry for isotope analysis. Fluxes of biogenic silica were calculated as for POC

232 using equation 1.

233 For Si isotope analysis, supernatants and reference materials ~~standards~~ were purified by passing
234 through ~~pre-cleaned~~ cation exchange columns (Bio-Rad AG50W-X12, 200-400 mesh resin) pre-
235 cleaned with HCl following (Georg et al.~~,~~ (2006) ~~using~~ ~~HCl as eluent~~. Samples were acidified to a pH
236 of 1-2 to ensure that all the silicon remained in solution. Samples were loaded onto columns and
237 eluted with Milli-Q water to produce a 2.5 ppm solution, and concentrations were checked to
238 confirm quantitative yields. Si isotopic composition was analysed within 24 hours of column
239 chemistry. Stable Si isotopic compositions were measured at the BIG laboratory on a Finnigan
240 Neptune Plus High-Resolution MC-ICP-MS (Thermo Fisher Scientific). The Si solutions were spiked
241 with magnesium spike (Inorganic Ventures MSMG-10 ppm), hydrochloric acid (1M HCl in-house
242 distilled) and sulphuric acid (0.1M H_2SO_4, ROMIL-UpA™ Ultra Purity Sulphuric Acid), and transferred
243 from the autosampler via a PFA Savillex C-Flow nebulizer (35 µl min^{-1}) connected to an Apex IR
244 Desolvating Nebulizer (Ward et al., 2022), and measured on the low-mass side to resolve any
245 isobaric interferences (e.g., $^{14}N^{16}O^{+}$). All standards and samples were blank-corrected offline. The
246 intensity of ^{28}Si in the 0.1M HCl blank was <1 % of the sample intensity in all sample runs.
247 Furthermore, we also measured Mg isotopes (^{24}Mg, ^{25}Mg and ^{26}Mg) as an internal isotopic reference
248 to correct for any mass-dependent fractionation (White et al., 2000). Measurements that resulted in
249 large corrections (>0.3 ‰ on δ^{30}Si) underwent repeat analysis. Instrumental mass bias was further
250 accounted for using a standard-sample bracketing method using a 2 ppm reference standard (NBS or
251 RM8546) solution. Two splits~~samples~~ were analysed for each sediment trap bottle ~~(pseudo replicates~~
252 ~~as the sediment trap material was heterogeneous)~~, as well as standards and sample blanks.
253 Solutions obtained from each split were measured in replicate (n = 2-3) alongside continuous
254 measurement of reference ~~standards~~ materials Diatomite and LMG-08 to ensure reproducibility and
255 to monitor data quality. Measurements of Diatomite and LMG-08 yielded δ^{30}Si of +1.23 ‰ (SD ±
256 0.03, n=18) and -3.40 ‰ (SD ± 0.05, n=5) respectively, which agreed with published values (Reynolds
257 et al., 2007; Hendry and Robinson, 2012; Grasse et al., 2017). Typical reproducibility between the
258 sediment trap sample splits (coming from the same sediment trap bottle) ~~ample~~ ~~pseudo replicates~~
259 was 0.034 ‰ (1 x SD). A lithogenic correction (e.g., Closset et al., 2015) was not carried out on these
260 samples. However, even an extreme scenario of variable lithogenic contamination of 1-5 % of
261 isotopically light marine clays (with δ^{30}Si of -2.3 ‰; Opfergelt and Delmelle, 2012) would only result
262 in a potential systematic offset of 0.12 ‰, which is an order of magnitude smaller~~less~~ than the
263 observed seasonal signal.

Chlorophyll and phytoplankton community composition

265 Surface chlorophyll concentrations were obtained from satellite-derived 8-day Ocean Colour CCI
266 (version 5.0) (Sathyendranath et al., 2021, 2019). We present the monthly mean of these 8-day data
267 for December at our study site (Figure 1), ~~We present the mean of 8-day concentrations for~~
268 ~~December 2018 as~~ as well as ~~the seasonal cycle of 8 day averaged chlorophyll concentrations~~ the 8-
269 day chlorophyll concentration data from September 2017 to December 2018 (Figure 2) averaged
270 over a 1 x 1° bounding box around our study site (-41 °W~~E~~, -40 °W~~E~~, -53 °S~~N~~, -52 °S~~N~~).

271 Light microscopy was used to assess ~~P~~phytoplankton and microzooplankton community composition
272 of a small selection of samples from the two main productive periods~~, were assessed via light~~
273 ~~microscope~~. A biological method of sample preparation and analysis was chosen, comparable with
274 Rembauville et al. (2015), to determine the quantity of empty and full cells. Following subsampling
275 using the rotary splitter, samples for morphological taxonomic analysis were diluted to a

standardised 25 ml. Samples were gently inverted using the Paul Schatz principle (figures of eight) for one minute to homogenise them, and 2 ml was withdrawn using a modified pipette with widened opening. Several common diatoms in Antarctic waters are long and slim; in particular, *Thalassiothrix antarctica* has been recorded with an apical axis up to 5mm. To ensure such specimens remain intact and are not excluded from the pipetting process, a wide bore opening is necessary. The 2 ml subsamples were used to fill a 1 ml Sedgwick Rafter counting chamber. Chambers were viewed using a compound light microscope (Nikon Eclipse 80i) with differential interference contrast at x200 magnification. For the larger, easily identifiable cells, the whole chamber was observed; for smaller cells a proportion of the chamber was examined depending upon cell abundance (at least 500 cells were counted). Only complete cells were enumerated to avoid over counting of fragmented specimens. Cells were determined as "full" or alive at time of collection if they possessed chloroplasts/plastids, pigment, a nucleus or, in the case of *Pronoctiluca*, a distinct accumulation body; cells lacking these internal features were deemed as "empty", or dead at time of collection. Specimens were identified according to Hasle and Syvertsen (1997); Medlin and Priddle (1990); Priddle and Fryxell (1985) and Scott and Marchan (2005).

Cell bio-volume and surface area estimates were calculated using geometrics and the appropriate shape-related equations for phytoplankton genera proposed by Hillebrand et al. (1999). Metrics used in the calculations were based on the average size of ten randomly selected specimens belonging to a species/taxonomic group within the samples.

3. Results

3.1. Environmental conditions

Mean current velocities were 0.11 (±0.06) and 0.06 (±0.03) m s^{-1} for shallow and deep current meters respectively (Supplementary Figure S1). Maximum current speeds recorded reached 0.43 and 0.18 m s^{-1} for shallow and deep meters respectively. The periods with currents substantially elevated above the mean were June for both traps, and additionally in late August/September for the shallow trap, both for periods of ~5-10 days. Both are periods of low fluxes during austral winter and are not the main subject of the study here, though it is likely that particle collection was biased at these times (Buesseler et al., 2007).

Satellite-derived estimates of surface chlorophyll show high concentrations during austral summer (January to March) peaking at 2.3 mg m^{-3}, as well as during spring (November-December), peaking at 2.1 mg m^{-3} (Figure 2, Figure S2). Data coverage is limited in the winter due to cloud cover, but concentrations appear to be <0.4 mg m^{-3}. We define here two productive periods (when chlorophyll concentrations were >0.4 mg m^{-3}), which we refer to throughout the manuscript, productive period 1: January to April 2018, and productive period 2: September to December 2018. We note that our sediment trap data begins on the 25th January so we do not capture the start of period 1.
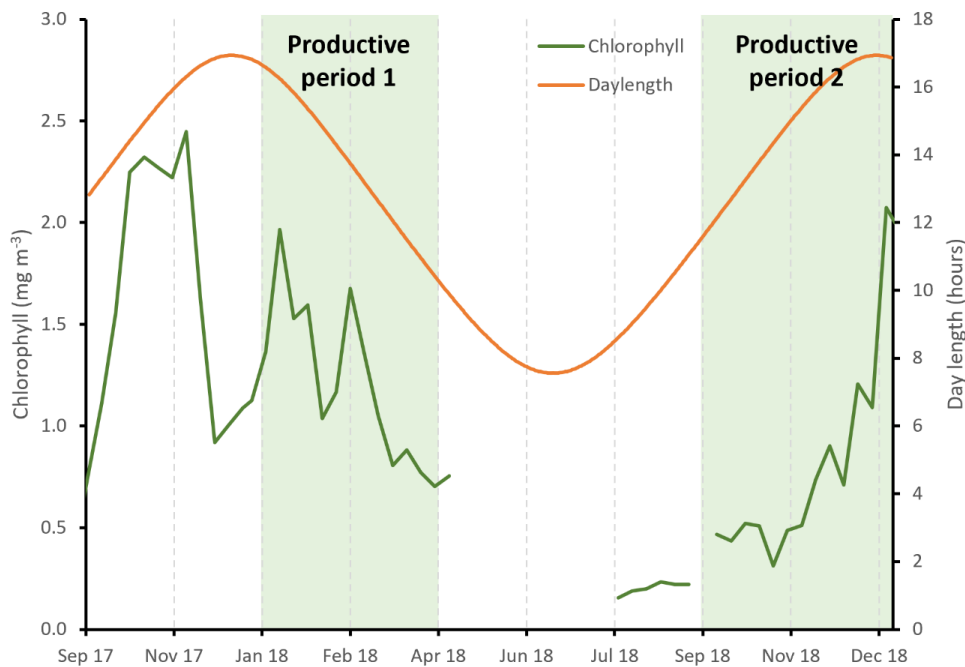
Figure 2: Seasonal cycle of satellite derived surface chlorophyll concentration (green line, 8-day data from the Ocean Colour CCI (version 5.0) (Sathyendranath et al., 2021, 2019)*). Daylength at -53 °SN is shown by the orange line. The two productive periods are highlighted by the shaded green region.*

3.2. POC, PN, BSi fluxes

There is a clear seasonal cycle in POC, PN and BSi fluxes, all tracking each other well (Figure 3). Since two to three splits were analysed from each sediment trap bottle, we refer here to the mean flux for each sediment trap bottle based on the available splits for that bottle. POC fluxes were low during austral autumn and winter, with mean fluxes <10 mg C m^{-2} d^{-1} and <7 mg C m^{-2} d^{-1} for shallow and deep traps respectively during the period March to October 2018. Higher fluxes were measured in summer 2018 (productive period 1), reaching means of 25.3 mg C m^{-2} d^{-1} in late January 2018 in the shallow trap and 13.1 mg C m^{-2} d^{-1} in late February in the deep trap. The maximum POC fluxes measured occurred in early December 2018 (productive period 2), reaching with mean POC fluxes of 45.7 mg C m^{-2} d^{-1} and 43.4 mg C m^{-2} d^{-1}, in shallow and deep traps respectively. PN fluxes follow the same trends as POC fluxes, peaking at 4.2 and 2.4 mg N m^{-2} d^{-1} during period 1, and 10.8 and 8.2 mg N m^{-2} d^{-1} during period 2, in shallow and deep traps respectively (Figure 3B). The mean POC:PN ratio (mol:mol) throughout the study period was 6.40 (± 0.73) and 6.02 (±0.90) in shallow and deep traps respectively with higher ratios in the productive periods compared to the winter months. Mean POC:PN ratios were 6.75 (±0.46) and 6.63 (±0.71) during period 1 and period 2 in the shallow trap, and 6.61 (±0.65) and 5.51 (±0.87) in the deep trap. Over the winter months POC:PN was 5.68 and 5.92 in shallow and deep traps respectively.

337 BSi fluxes (Figure 3C) track those of POC well. Lowest fluxes (<20 mg SiO$_2$ m^{-2} d^{-1}, except a small peak

338 of up to 39.7 mg SiO$_2$ m^{-2} d^{-1} in May 2018) occurred in the autumn/winter (March-October). During

339 summer 2018 (productive period 1), BSi fluxes were high, reaching ~~mean fluxes of~~ 129.1 mg SiO$_2$ m^{-2}

340 d^{-1} in early February in the shallow trap and~~,~~ 84.3 mg SiO$_2$ m^{-2} d^{-1} in late February in the deep trap. By

341 far the highest fluxes were observed in spring 2018 (productive period 2), peaking in early December

342 at ~~a mean of~~ 562.4 mg SiO$_2$ m^{-2} d^{-1}, and 285.4 mg SiO$_2$ m^{-2} d^{-1} in shallow and deep traps respectively.

343 The mean BSi:POC ratio (mol:mol) throughout the study period was 29.82 (± 17.80) and 25.86

344 (±11.72) in shallow and deep traps respectively. Higher BSi:POC ratios were observed in the shallow

345 trap in period 1 (38.45 ±10.96), and both shallow and deep traps in period 2 (36.94 ±16.32 and 35.70

346 ±12.10 respectively). BSi:POC ratios were lower in the deep trap during period 1 (23.64 (±6.82).

347 The match in timing of ~~sharp peaks~~elevated fluxes ~~of~~in POC, PN and BSi fluxes in the shallow and

348 deep traps in spring (period 2) highlights that sinking rates must be sufficient (>114 m d^{-1}) for

349 particles to travel the 1600 m between the two traps in the 14 day period that th~~at~~ose sediment

350 trap cups w~~as~~ere open. In period 1, there was a time lag of 14 to 35 days ~~(based on the sampling~~

351 ~~duration of each sample bottle was open)~~ between the timing of the maximum POC, PN, and BSi

352 fluxes in the deep and shallow sediment traps. This suggests sinking rates of 46-114 m d^{-1}. However,

353 we stress that this assumes vertical sinking, which as we discuss in ~~the~~ Section 4 is not always the

354 case.
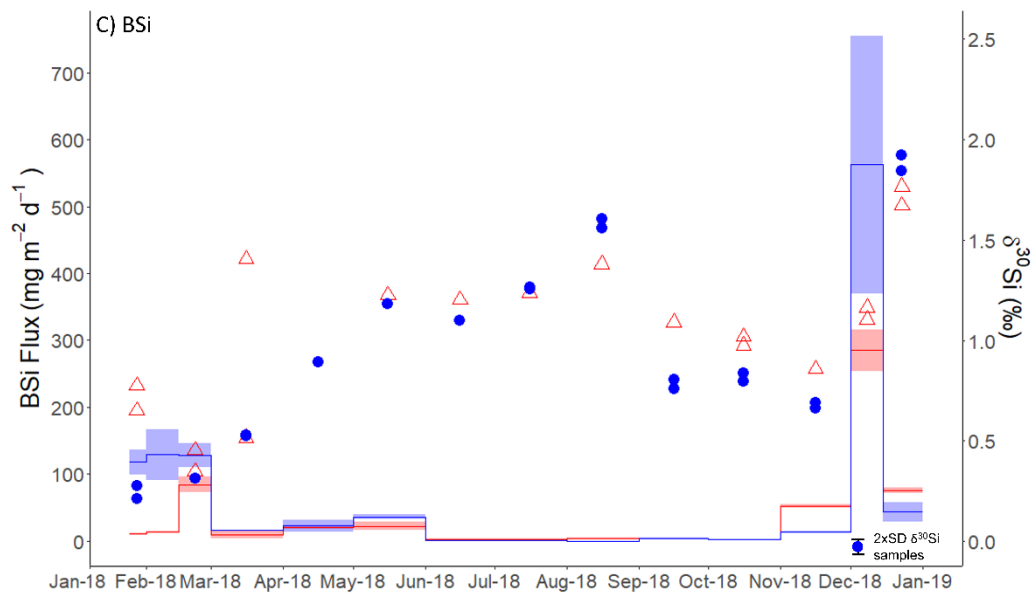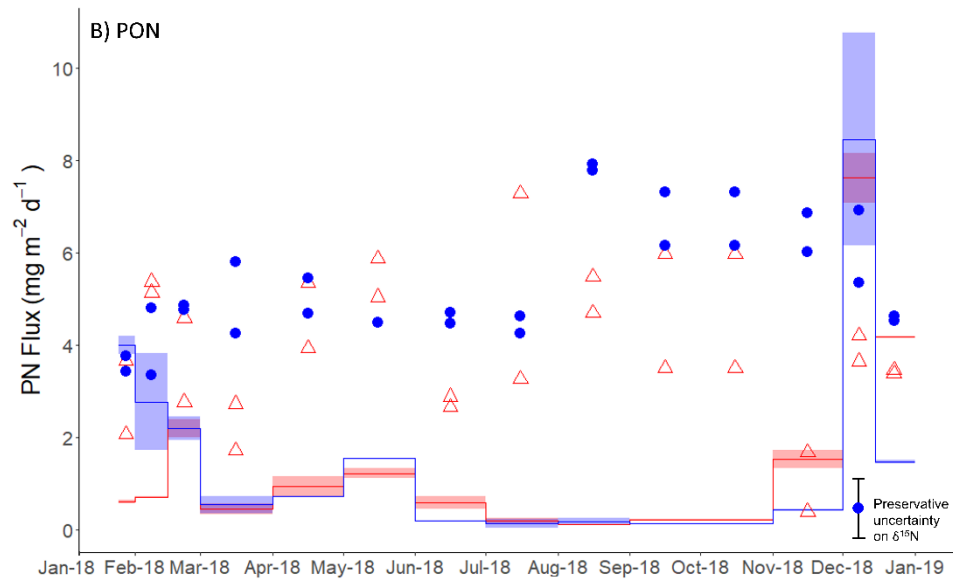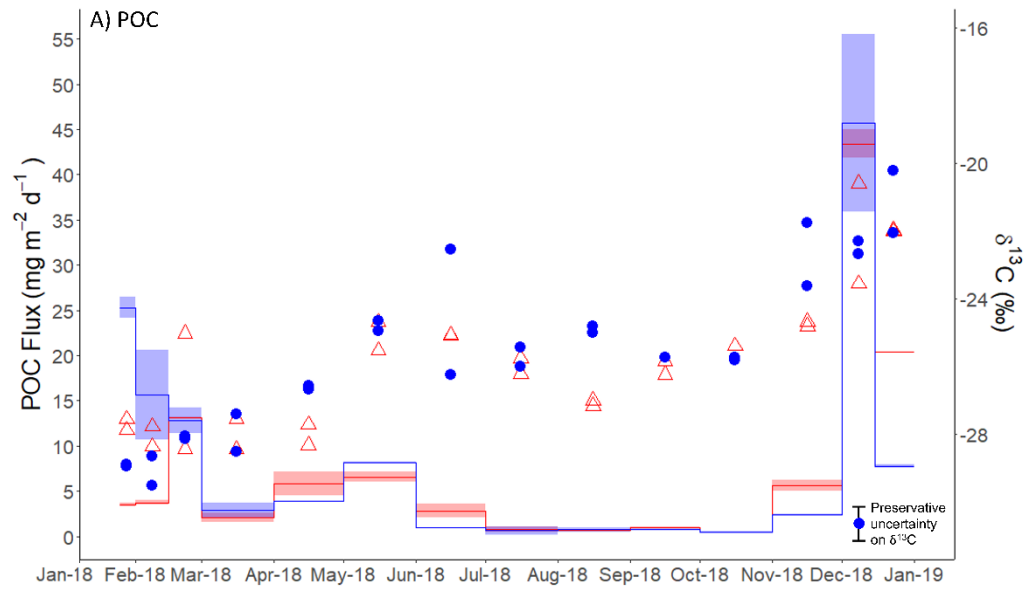
Figure 3: A) Particulate organic carbon (POC), B) particulate nitrogen (PN) and C) biogenic silica (SiO$_2$, BSi) fluxes (mg m^{-2} d^{-1}) at deep (red shading) and shallow (blue shading) sediment traps. Shading indicates the maximum and minimum flux from two ~~replicate~~splits ~~samples~~, with the solid line indicating the mean value. Coloured points show isotope ratios for A) δ^{13}C$_{POC}$, B) δ^{15}N$_{PN}$ and C) δ^{30}Si$_{BSi}$ with red open triangles and blue filled circles indicating deep~~shallow~~ and shallow~~deep~~ sediment traps, respectively. The maximum error on sediment trap δ^{13}C$_{POC}$ (±1 ‰) and δ^{15}N$_{PN}$ (±1.5 ‰) values are shown by scaled error bars in the bottom right corner, and are associated with formaldehyde preservation (Mincks et al., 2008) since this vastly exceeds analytical error. For δ^{30}Si$_{BSi}$, the scaled error bar represents 2 x SD (‰ 0.7) for the analytical sample replicates. For each sample, ~~fluxes and~~ isotope ratios are given at the midpoint of the period ~~date~~ that the sample cup was open~~ed~~.

3.3. δ^{13}C$_{POC}$, δ^{15}N$_{PN}$ and δ^{30}Si$_{BSi}$ Isotopes

δ^{13}C$_{POC}$ values of deep and shallow sediment trap samples track each other well and show the same order of enrichment and ~~/~~depletion (Figure 3A). Again, when presenting the results for an individual sediment trap bottle, we give the mean of replicate splits from that sediment trap bottle unless otherwise stated. Initially, from January to March 2018, we see isotopically light ~~mean~~ δ^{13}C$_{POC}$ values between -27.40 and -28.56 ‰, before increasing to -24.38 ‰ and -25.07 ‰ in June in shallow and deep traps respectively. Over winter, δ^{13}C$_{POC}$ became more depleted (shallow: -25.76 ‰ in October, deep -27.07 ‰ in August) with a slight divergence (2.17 ‰) in the tracking of deep and shallow δ^{13}C$_{POC}$ in August 2018. Coinciding with increasing chlorophyll concentrations, δ^{13}C$_{POC}$ became more enriched during the period September to December 2018 (-25.72 to -21.13 ‰ and -26.04 to -21.98 ‰ for shallow and deep traps respectively).

Comparison of flux-weighted δ^{13}C$_{POC}$ values confirms the carbon isotopic similarity of deep and shallow traps, particularly during period 2 (Table 1). These results also highlight the ~~baseline~~ shift in both δ^{13}C$_{POC}$ and δ^{30}Si$_{BSi}$ between period 1 and period 2.

Table 1: Sediment trap seasonal (Jan 2018-Dec 2018), period 1 (Jan 2018 – April 2018), and period 2 (Sept 2018-Dec 2018) flux-weighted mean δ^{13}C$_{POC}$ (‰), δ^{15}N$_{PN}$ (‰) and δ^{30}Si$_{BSi}$ (‰) for shallow (400 m) and deep (2000 m) traps. Given that the analytical conditions were the same for all samples measured, we use the pooled variance over the applicable time period as a measure of uncertainty on these mean isotopic ratios. D~~,~~egrees of freedom (dof) are based on cups with replicate isotopic measurements and are given in parentheses. ~~Maximum errors are based on uncertainty associated with formaldehyde preservative and analytical sample replicate~~

Time period	δ^{13}C$_{POC}$ (‰)		δ^{15}N$_{PN}$ (‰)		δ^{30}Si$_{BSi}$ (‰)	
	Shallow	Deep	Shallow	Deep	Shallow	Deep
Seasonal	-25.15 ±0.49 (dof=14)~~1‰~~	-24.40 ±0.45 (dof=14)~~‰~~	2.07 ±0.34 (dof=14)~~1.5‰~~	0.39 ±0.43 (dof=14)~~1.5‰~~	0.50 ±0.09 (dof=8)~~7‰~~	0.86 ±0.10~~0~~ (dof=6)~~7‰~~
Period 1	-28.30 ±0.31~~1~~ (dof=5)~~‰~~	-27.52 ±0.33 (dof=5)~~1‰~~	1.16 ±0.36 (dof=5)~~1.5‰~~	0.73 ±0.58 (dof=5)~~1.5‰~~	0.25 ±0.09 (dof=2)~~7‰~~	0.47 ±0.13~~0~~ (dof=2)~~7‰~~

| Period 2 | -22.47 ±1.03 (dof=5)‰ | -22.79 ±0.74 (dof=5)1‰ | 2.97 ±0.66 (dof=5)1.5‰ | -0.09 ±0.65 (dof=5)1.5‰ | 1.54 ±0.300 (dof=4)7‰ | 1.08 ±0.140 (dof=4)7‰ |

$\delta^{15}N_{PN}$ values are less consistent between deep and shallow sediment trap samples and there is more heterogeneity between sample splitreplicates. For the shallow trap we see values ranging between +0.13 and +2.96 ‰ (mean +1.42 ‰, SD 0.79 ‰) from January to June 2018, and, for the deep trap, values ranged between -1.95 and +3.04 ‰ (mean +0.60 ‰, SD 1.60 ‰) during this period. There is no clear trend during this period, but shallow and deep traps have δ15NPN of similar magnitude. Values increase between June and August, reaching a mean of +5.42 and +2.10 ‰ in shallow and deep traps respectively. From August to December (shallow), and August to November (deep), we see a trend of decreasing $\delta^{15}N_{PN}$ to +1.49 and -2.77 ‰ in shallow and deep traps respectively, with the decrease being of similar magnitude (3.93 and 4.87 respectively) for both traps. Shallow $\delta^{15}N_{PN}$ are consistently higher than deep $\delta^{15}N_{PN}$ by 4.52 ‰ on average during this period (August to November). In the deep trap we see a final increase in $\delta^{15}N_{PN}$ coinciding with the increase in PN flux from November to December 2018, reaching a mean of +0.71 ‰. The same increase in $\delta^{15}N_{PN}$ is not apparent in the shallow trap.

Si isotope compositions in deep and shallow samples were similar, exhibiting the same seasonal patterns. Both deep and shallow traps showed an increase in $\delta^{30}Si_{BSi}$ from January to July 2018 (+0.24 to +1.26 ‰) with the steepest increase occurring from March to May (Figure 3C). Sample splitsreplicates generally showed good agreement with one exception during March 2018 when duplicate samplessample splits from the deep sediment trap were +0.52 and +1.41 ‰, highlighting the heterogeneous nature of the sediment trap material. Isotopic values were then quite steady over winter until the end of August when $\delta^{30}Si_{BSi}$ began to decrease steeply, reaching +0.68 and +0.86 ‰ in shallow and deep traps respectively in November 2018. Following this, $\delta^{30}Si_{BSi}$ increased rapidly to +1.72 (deep) and +1.89 ‰ (shallow) coinciding with the large increase in BSi fluxes at this time.

3.4. Phytoplankton community structure

Eight samples (four deep and four shallow, table 2) were analysed by light microscopice ally for phytoplankton composition to cover the high productivity periods 1 and 2. Diatoms, silicoflagellates and dinoflagellates were observed, with a dominance of diatoms. Micro-zooplankton were also recorded, in particular radiolarian and tintinnids, though these were not dominant by biovolume or abundance. OOnly intact cells were identified and counted. In terms of abundance, during period 1, the diatoms *Fragilariopsis spp.* dominated both deep (58-66 %) and shallow (~70 %) trap samples (Figure 4A, CB), whereas during period 2 the phytoplankton community structure was more mixed with contributions from the diatoms *Thalassionema nitzshiodes, Chaetoceros,* small (<20 μm) centrics, as well as *Fragilariopsis spp.* Large centric diatoms (>20 μm) represented 15-20 % of the community by abundance in the deep trap during productive period 1, but <2.5 % in productive period 2. Interestingly we do not see these large centrics in the shallow trap during productive period 1, implying that sinking velocities were < 76 m d^{-1} for these large phytoplankton cells based on the duration that the first sediment trap bottle was open and the depth between the two traps.

In terms of biovolume, *Fragilariopsis spp.* were still a dominant component of the shallow trap sample in period 1 (~33 %) but were <9 % of the community in the deep trap during period 1, with

429 the large cells of the diatom *Coscinodiscus* dominating 39-67 % (Figure 4BC, D). Diatoms, *Corethron*
430 *pennatum* (shallow: 10-13 %; deep: 15 %), *Rhizosolenia* (shallow: 9-21 %), and large centric diatoms
431 (>20 μm) (shallow: 10-17 %; deep: 16-20 %), as well as the silicoflagellatend *Dictyocha* (shallow: 9-10
432 %; deep: 8 %), were also relatively high in terms of biovolume during period 1. During period 2, the
433 community in terms of biovolume was quite mixed in the shallow trap (Figure 4BC), with similar
434 contributions from *Fragilariopsis spp.* (22-28 %), *Dictyocha* (14-15 %), *Coscinodiscus* (10 %), and,
435 small (<20 μm, 9-14 %) and large (>20 μm, 9-19 %) centric diatoms (>20μm, 9-19%) in the deep trap.
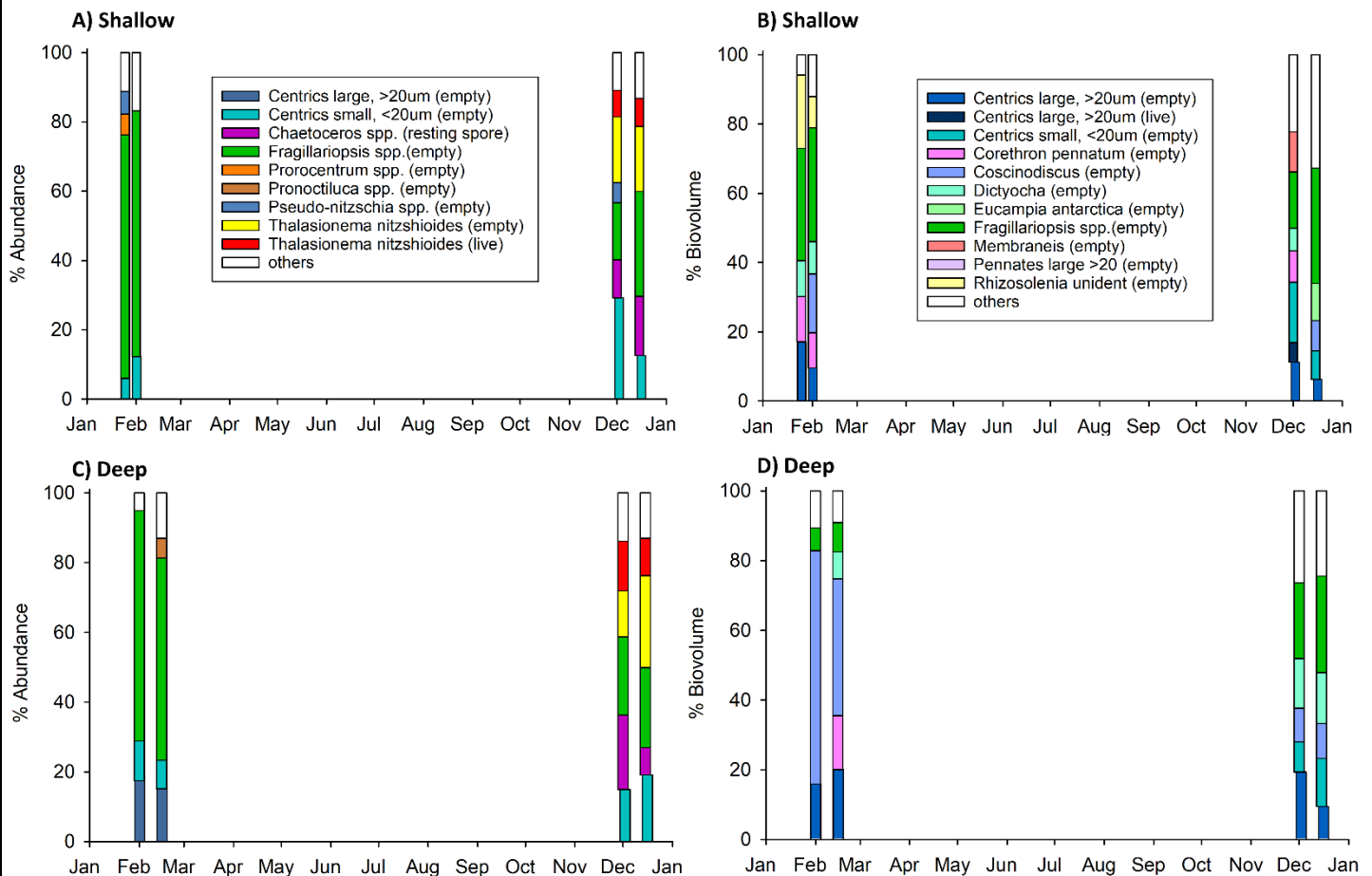
Figure 4: Phytoplankton assemblage of A,B) shallow and C, D) deep sediment trap samples, according to abundance (A, C) and biovolume (CB, D). Four samples were taxonomically identified for each trap. Shown here are the Plots A and CB show phytoplankton contributing >5 % by abundance, and (A,B) or plots BC and D show >5 % by biovolume (C,D). Four samples were taxonomically identified taxonomically for each trap. Note that only intact cells were counted.

442

4. Discussion

In this study we measure the seasonal cycle of POC, PN and BSi fluxes as well as the $\delta^{13}C_{POC}$, $\delta^{15}N_{PN}$ and $\delta^{30}Si_{BSi}$ values of sinking particles collected in shallow (400 m) and deep (2000 m) sediment traps in the Scotia Sea, Southern Ocean. Both the magnitude and isotopic compositions were generally similar in the shallow and deep sediment traps, suggesting that most remineralisation occurred in the upper 400 m. This highlights that material reaching 400 m likely facilitates the transfer of carbon much deeper in the ocean, sequestering carbon for longer time periods (Kwon et al., 2009).

4.1. Seasonal flux cycles

The Sseasonal cycles of POC agree well with previously published work at the same location (Manno et al., 2015), with peaks in austral spring and late summer,; though the peak POC fluxes recorded here (means of 45.7 mg C m^{-2} d^{-1} and 43.4 mg C m^{-2} d^{-1}, in shallow and deep traps respectively) are higher than those observed in previous years (22.9 mg C m^{-2} d^{-1}; Manno et al., (2015)). A smaller additionalthird peak in POC flux (<10 mg C m^{-2} d^{-1}) occurred in April/May, in agreement with some previous years (Manno et al., 2015). PN fluxes followed the same seasonal trend as POC for both deep and shallow traps suggesting a similar source. The similar magnitude of POC:PN ratios in period 1 in the two traps support consistency in the degree of degradation at these depths. The lower POC:PN ratios measured in the deep trap between August and October, compared to the shallow trap are consistent with a divergence in $\delta^{15}N_{PN}$ ratios, and could relate to a change in source material and/or degradation state between the two traps at this time.

Our measured The fluxes of BSi observed here are higher than previously observed at this site at 2000 m in 2012 (Rembauville et al., 2016). Maximum fluxes of 46.0 mg SiO$_2$ m^{-2} d^{-1} were recorded by Rembauville et al. (2016) in January 2012, which though of similar magnitude to our summer peak of 84.3 mg SiO$_2$ m^{-2} d^{-1}, is an order of magnitude lower than the spring peak of 285.4 mg SiO$_2$ m^{-2} d^{-1} in December 2018. However, the Rembauville et al. (2016) record ends in November and therefore would not have captured the main peak in particle flux following the phytoplankton spring bloom in December (apparent in satellite surface chlorophyll, Figure 2 in Rembauville et al., (2016)). Additionally, we do not capture the first 3 weeks of January in our data. Closset et al. (2015) measured very high fluxes (>700 mg SiO$_2$ m^{-2} d^{-1}) of BSi south of the Polar Front in the Australian sector of the Southern Ocean at 2000 m, and similarly high fluxes have been observed in other sectors (Fischer et al., 2002; Honjo et al., 2000).

We define two main productive periods, productive period 1 from January to April 2018, and productive period 2 from September to December 2018 when chlorophyll concentrations were >0.4 mg m^{-3}. Satellite data suggest the magnitude of chlorophyll concentration was similar during both productive periods, but increasing in magnitude throughout period 2, and decreasing in period 1, consistent with timing of sampling. The particle fluxes associated with productive period 2 were much higher than those during productive period 1, a difference which is particularly pronounced for BSi fluxes. The bloom during period 2 was more geographically widespread (Figure S2) and thus it is possible that if more of the material reaching the trap was sourced from productive waters, this could have supported the higher fluxes observed at this time. The observed higher BSi fluxes in productive period 2 could also relate to the presence of more heavily silicified diatom species at this time, including the occurrence of resting spores (*Chaetoceros spp.*; Figure 4, and Rembauville et al. (2016)), increased aggregation (and thus sinking) potential, higher sinking rates, and/or reduced

485 grazing pressure. The fact that we observed resting spores at the end of productive period 2,

486 suggests that nutrients may have started to become limiting for at least some of the phytoplankton

487 community (e.g. silicic acid and/or iron, (Rembauville et al., 2016)). ~~Satellite data suggest the~~

488 ~~magnitude of chlorophyll concentration was similar during both productive periods, but increasing in~~

489 ~~magnitude throughout period 2, and decreasing in period 1.~~ POC and BSi fluxes track each other

490 closely and ratios suggest high export of biogenic silica (Figure 5). This, ~~, which,~~ combined with our

491 visual observations of a dominance of algal material in the trap during the spring peak that was

492 ~~(~~dominated by diatoms ~~,~~ (Figure 4), ~~highlight~~suggest an important role for ~~s the role of~~ diatoms in

493 transferring organic carbon to the deep ocean at this time. This could be achieved if cells are large

494 through large mineral (silica) ballasted cells sinking at high velocities (Baumann et al., 2022), ~~their~~

495 ~~greater density, and thus sinking velocities, associated with mineral (silica) ballast,~~ or through the

496 bioprotection of internal organic matter from grazing and oxidation by~~of~~ the diatom silica frustules

497 (Passow and De La Rocha, 2006; Armstrong et al., 2001; Smetacek et al., 2004).

498 *4.2. Seasonal variation~~shift~~s in isotope ratios*

499 In terms of the seasonality, we see broadly similar trends for both $\delta^{13}C_{POC}$ and $\delta^{30}Si_{BSi}$ (linear

500 regression, $R^2 = 0.452$, p~~P~~<0.001, Figure 5), again highlighting the close coupling of carbon and silicon

501 cycling processes. We do not find significant relationships between $\delta^{15}N_{PN}$ and $\delta^{13}C_{POC}$ or $\delta^{30}Si_{BSi}$. We

502 break the season into 3 main periods for discussion, productive period 1 (first export event), the

503 winter flux hiatus, and productive period 2 (second export event).
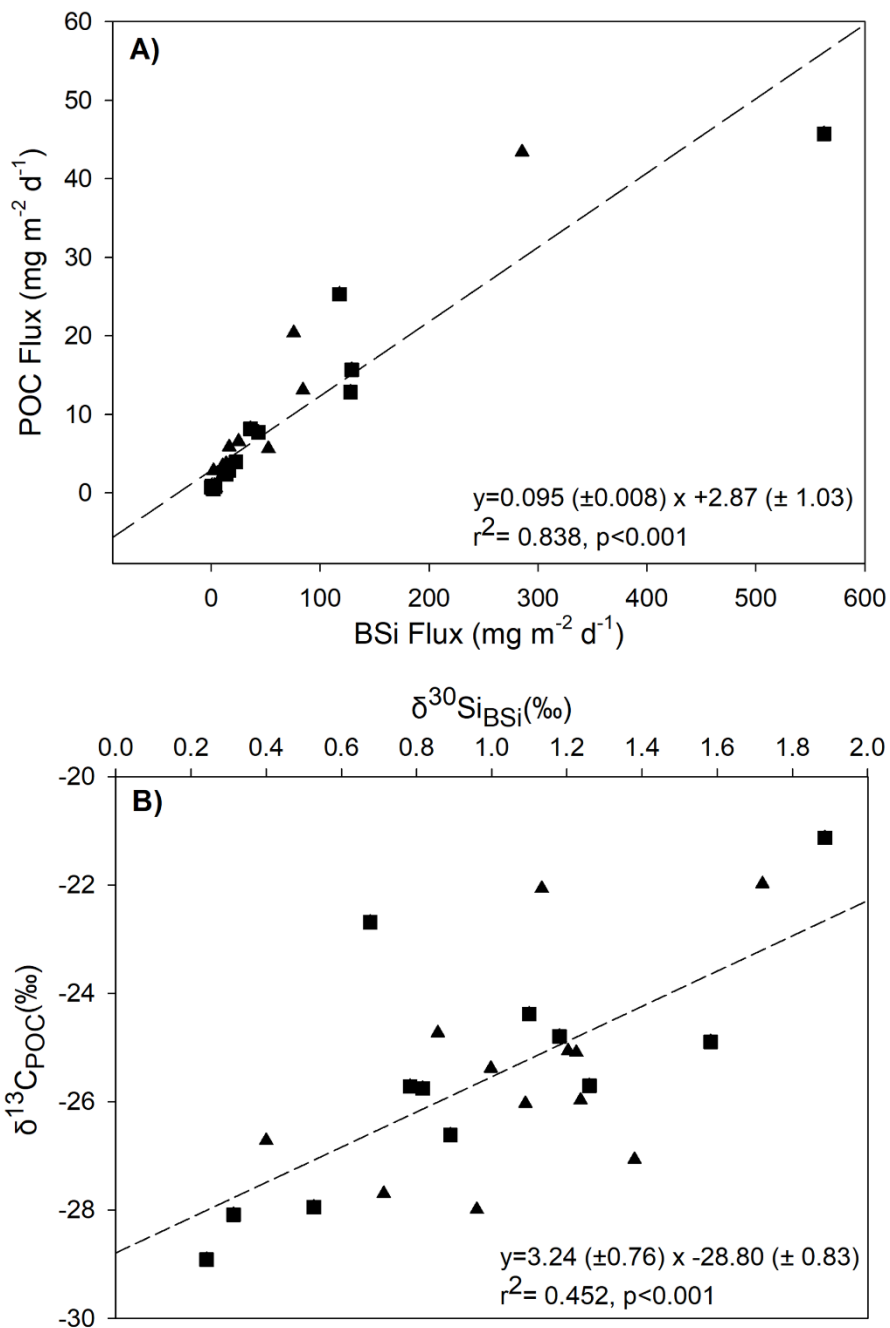
504

505 *Figure 5: Relationship between BSi and POC for data from both deep (triangles) and shallow*
506 *(squares) sediment traps. A) Regression between BSi and POC fluxes, and B–) between $\delta^{13}C_{POC}$ and*
507 *$\delta^{30}Si_{BSi}$. Regression lines are shown by dotted lines with coefficients and associated standard errors*
508 *also shown.*

509

510 *4.2.1. Productive period 1*

511

In terms of the seasonality, we see broadly similar trends for both $\delta^{13}C_{POC}$ and $\delta^{30}Si_{BSi}$ (linear regression, $R^2 = 0.452$, P<0.001), again highlighting the close coupling of carbon and silicon cycling processes. During productive period 1, $\delta^{13}C_{POC}$ is low, averaging -28.30 and -27.52 ‰ in shallow and deep traps respectively, close to that expected for Southern Ocean phytoplankton employing typical C3 metabolism (i.e. diffusive CO_2 transfer into the internal cell pool and Rubisco carboxylation) (Raven, 1997). This is supported byconsistent with the dominance of diatoms (*Fragilariopsis spp.*) in the trap material, as Bacillariophyceae are known to employ C3 metabolism (Table IV in Raven, 1997). Preferential uptake of ^{28}Si by diatoms (De La Rocha et al., 1997) during the late spring bloom of productive period 1, also explains the low $\delta^{30}Si_{BSi}$ values. BSi:POC ratios were elevated at the start of productive period 1, suggesting that phytoplankton were heavily silicified. After initial low values, we see a progressive increase in both $\delta^{13}C_{POC}$ and $\delta^{30}Si_{BSi}$, reflecting the progressive utilisation of both ^{12}C and ^{28}Si as nutrient pools are consumed during the bloom. As such, the diatom cells reaching the sediment trap in late spring/summer were utilising increasingly isotopically-enriched C and Si for growth leading to progressive isotopic enrichment of the cells sinking into the sediment trap. This observation fits with elevated but decreasing surface chlorophyll concentrations from February to April 2018. Increasing $\delta^{13}C_{POC}$ and $\delta^{30}Si_{BSi}$ into the late summer may also partially reflect preferential remineralisation of the more labile ^{12}C and ^{28}Si in particles as they sink through the upper 400 m of the water column. T Though the lack of variation in $\delta^{13}C_{POC}$ and $\delta^{30}Si_{BSi}$ between 400 and 2000 m in our study suggests this may be limited over these depth ranges, or that there is no fractionation effect. Whilst laboratory-based silica dissolution experiments are equivocal (Demarest et al., 2009; Wetzel et al., 2014), our findings agree with field studies that also indicate a lack of Si isotopic fractionation during diatom silica dissolution (Closset et al., 2015; Egan et al., 2012).

During the summer autumn period (January- June 2018)productive period 1, there was no clear trend in $\delta^{15}N_{PN}$, with values between -1.954 and +23.9604 ‰. We speculate that this mixed signal with no significant difference between deep and shallow traps resulted from a combination of surface phytoplankton using both ammonium and nitrate as the inorganic nitrogen source, and variability in the sediment trap material composition., for example the presence of faecal pellets, as well as animal moults and carcasses. Enrichments of 2-4 ‰ occur between successive trophic levels, and egestion and excretion can have varying isotopic effects (see Section 4.3), thus the presence of faecal pellets, animal moults and carcasses could alter the isotopic composition of the sediment trap material. Additionally, any supply of ammonium through remineralisation would be utilised quickly because ammonium is kinetically favourable to nitrate (Glibert et al., 2016), resulting in particles with a decreased $\delta^{15}N_{PN}$ compared to those produced by nitrate assimilation.

4.2.2. Winter hiatus

Between May and August, both $\delta^{13}C_{POC}$ and $\delta^{30}Si_{BSi}$ showed little changewere consistent, with a slight progressive decrease for $\delta^{13}C_{POC}$ and slight increase in $\delta^{30}Si_{BSi}$. It is possible that the slight progressive trend towards a lighter carbon isotopic composition of sinking particles from -24.94 to -25.98 ‰ is driven by a mixture of older, isotopically heavier particles that have undergone partial remineralisation and the input of fresher material of different isotopic composition from the small secondary peak in POC we observed in April/May. An input of smaller, more slowly sinking cells reaching the trap in increasing numbers following the initial late spring peak in production could drive the lower $\delta^{13}C_{POC}$ at this time. Additionally, the pulse of material could be driven by a

successive peak in production of a different phytoplankton community with a different isotopic signature. ~~Either the small autumn peak consisted of a different phytoplankton community, or we are seeing a signal of smaller, more slowly sinking cells reaching the trap in increasing numbers following the initial late spring peak in production.~~ Korb et al. (2012) found an increasing presence of dinoflagellates from spring to summer, as well as seasonal changes in the size structure of the phytoplankton community to the northwest of South Georgia, supporting either hypothesis. We do not have the species composition data from this time period to evidence this directly, but we suggest that the reduction in $\delta^{13}C_{POC}$ does not relate to a mixing event and a resupply of ^{12}C, due to the fact that $\delta^{30}Si_{BSi}$ continued to increase slowly. Given the generally lighter silicon isotopic composition of seawater below the photic zone, we would expect a mixing event to also result in a decline in seawater $\delta^{30}Si$ and consequently~~, so,~~ $\delta^{30}Si_{BSi}$. This would mean that our hypothesised shift in phytoplankton species composition in the traps (May-August) did not impact Si fractionation to the same extent as carbon isotopes. Whereas size, growth rates, cell geometry and different carbon acquisition mechanisms have all been highlighted as impacting the $\delta^{13}C_{POC}$ of marine plankton (Popp et al., 1999, 1998; Bidigare et al., 1999; Trull and Armand, 2001; Tuerena et al., 2019), species dependent Si fractionation by polar and subpolar diatoms has only been observed in the laboratory, not in the field (Annett et al., 2017; Cassarino et al., 2017; Sutton et al., 2013).

$\delta^{15}N_{PN}$ in the shallow trap showed a slight progressive decrease over the winter period, before increasing in August to 5.42 ‰. The progressive decrease is consistent with the propagation of the surface signal of phytoplankton growth and fractionation, with increasing influence of ammonium uptake as the season progresses that leads to low $\delta^{15}N_{PN}$. The large range in $\delta^{15}N_{PN}$ in the deep trap in July makes it difficult to determine with certainty a trend in $\delta^{15}N_{PN}$ in the deep trap between July and October.

~~*Figure 5:*~~

~~Between May and August, both $\delta^{13}C_{POC}$ and $\delta^{30}Si_{BSi}$ were consistent, with a slight progressive decrease for $\delta^{13}C_{POC}$ and slight increase in $\delta^{30}Si_{BSi}$. It is possible that the slight progressive trend towards a lighter carbon isotopic composition of sinking particles from -24.94 to -25.98‰ is driven by a mixture of older, isotopically heavier particles that have undergone partial remineralisation and the input of fresher material from the small secondary peak in POC we observed in April/May. Either the small autumn peak consisted of a different phytoplankton community, or we are seeing a signal of smaller, more slowly sinking cells reaching the trap in increasing numbers following the initial late spring peak in production. Korb et al. (2012) found an increasing presence of dinoflagellates from spring to summer, as well as seasonal changes in the size structure of the phytoplankton community to the northwest of South Georgia, supporting either hypothesis. We do not have the species composition data from this time period to evidence this directly, but we suggest that the reduction in $\delta^{13}C_{POC}$ does not relate to a mixing event and a resupply of ^{12}C, due to the fact that $\delta^{30}Si_{BSi}$ continued to increase slowly. Given the generally lighter silicon isotopic composition of seawater below the photic zone, we would expect a mixing event to also result in a decline in seawater $\delta^{30}Si$ and, so, $\delta^{30}Si_{BSi}$. This would mean that our hypothesised shift in phytoplankton species composition~~

612   *4.2.3. Productive period 2*

613 At the start of productive period 2 (September)Between August and September we saw a
614 significantharp decrease in $\delta^{30}Si_{BSi}$ (~0.5 ‰) in both traps suggesting resupply of ^{28}Si enriched silicic
615 acid to the euphotic zone via mixing. Interestingly, we did not see the same consistent shift in
616 carbon isotopes; we measured a ~1 ‰ decrease in the shallow trap $\delta^{13}C_{POC}$ and a ~1 ‰ increase in
617 the deep trap $\delta^{13}C_{POC}$. We speculate that this mixing could bring waters of increased silicic acid
618 concentrations to the surface, promoting full expression of the isotope fractionation effect enabling
619 fractionation from phytoplankton uptake andsupporting thus lower $\delta^{30}BSi_{BSi}$ in sinking particles. To
620 match our observations, these mixed waters would need to be following phytoplankton uptake, but
621 that the mixed waters were similar in dissolved inorganic carbon concentrations and $\delta^{13}C$, which.
622 This could relate to the depth of mixing and differences in the depth at which POC and BSi are
623 remineralised (Friedrich and Rutgers van der Loeff, 2002; Weir et al., 2020). We note that current
624 velocities recorded at this time were elevated (Figure S1), particularly in the deep trap, suggesting a
625 shift in the surrounding velocity fields, which and may also have resulted in biased sample collection
626 at this time through either over or under collection (Buesseler et al., 2007). Whereas $\delta^{13}C_{POC}$
627 progressively increased during productive period 2, from -25.88 ‰ in September to -21.56 ‰ at the
628 end of December (mean of deep and shallow traps), $\delta^{30}Si_{BSi}$ continued to decrease until November
629 before showing a sudden increase from +0.74 ‰ to +1.80 ‰ at the end of the sampling period. This
630 may suggest that DSi, (or co-limiting nutrients,) was replete, and uptake could occur unhindered
631 until November 2018 when very high rates of production and the associated high fluxes of BSi
632 increased the demand for DSi, and led to enrichment of $\delta^{30}Si$ in overlying waters and subsequently
633 sinking siliceous phytoplankton. For carbon, uptake was sufficient from September 2018 to
634 progressively deplete source waters (and subsequent newly formed phytoplankton cells) in ^{12}C,
635 driving an increase in $\delta^{13}C$ in surface waters and newly formed phytoplankton cells. BSi:POC ratios
636 increased from September to December suggesting that material reaching the traps was increasingly
637 silicified.

638 δ15NPN decreased progressively from August to DecemberThe progressive decrease is consistent with
639 the propagation of the surface signal of phytoplankton growth and fractionation, with increasing

20

Interestingly, unlike C and Si isotopes, we saw a divergence in the nitrogen isotopic composition of deep and shallow traps ~~during this period~~between August and December. ~~Though they mostly followed the same decreasing trend, the trend in the shallow trap was less pronounced and started from a higher mean value of +5.42‰.~~ The sharp increase in mean $\delta^{15}N_{PN}$ from +1.32 ‰ in July to +5.42 ‰ in August 2018 in the shallow trap that initiated the divergence strongly suggests an advective change in source material. As noted above, this was a period of increased horizontal velocities and may have facilitated material reaching the two traps from different sources of differing initial composition and degradation states. The substantially lower $\delta^{15}N_{PN}$ in the deep trap from August to November, compared to that of the shallow trap is surprising. It would be expected, that, as particles sink and are progressively decomposed this would ~~given that we would expect progressive decomposition of particles to~~ remove dissolved nitrogen depleted in ^{15}N, thus increasing. ~~This would increase~~ $\delta^{15}N_{PN}$ in the particles~~., and i~~Indeed many studies have observed this trend of increasing $\delta^{15}N$ with depth in suspended particles (Altabet et al., 1991 and references ~~within~~therein). However, like Altabet et al. (1991), we observe lower $\delta^{15}N_{PN}$ in sinking particles in the deep sediment trap. This has also been observed previously in Antarctic waters (Wada et al., 1987). Though the reason for this is not well understood (Sigman and Fripiat, 2019), it appears to be a consistent phenomenon. Particles in our deep trap must therefore be gaining light nitrogen or losing heavy nitrogen and could reflect a different source composition. In agreement with Altabet et al. (1991), we suggest that lateral transport of low $\delta^{15}N_{PN}$ from a region of increased ammonium--based production could explain this, highlighting a difference in the source of sinking particles to the two traps. Altabet et al. (1991) also suggests that, since protein nitrogen is 3 ‰ higher than bulk nitrogen, the selective decomposition of protein could explain the decrease in $\delta^{15}N$ with depth, though why this would not be the case also for suspended PN is unclear. We observe the greatest divergence in shallow and deep N isotope compositions during periods of low PN flux (Figure 3), consistent with the observations of Altabet et al. (1991), enabling a low flux of laterally supplied material to have an amplified impact on the isotope signal. In support of this, in December when particle fluxes increase sharply with the spring bloom, $\delta^{15}N_{PN}$ in the deep trap increases more in line with that of the shallow trap, highlighting a switch from source material being dominated by lateral supply when vertical supply is negligible, to the dominance of vertical supply from surface production following the phytoplankton bloom.

~~Though complex, it is clear that seasonal patterns in isotopic composition of particulate material reaching the sediment traps closely reflects the degree and type of nutrient utilisation in the source waters. As we capture two main productive periods in our study, we can more closely examine the different isotopic baselines observed in these two periods.~~

~~4.2.~~4.3. Drivers of a shifting isotopic ~~baseline~~ratios

The mean flux-weighted isotopic composition measured during ~~P~~productive periods 1 (January to April 2018) and 2 (September to December 2018) suggests that the processes driving the flux of material at these times differ ~~exhibit differing baselines in their isotopic composition~~ (Figure 3, Table 1). The divergence in the $\delta^{15}N_{PN}$ of deep and shallow trap material during period 2 limits our ability

to compare the temporal shifts in mean isotopic ratiobaselines for nitrogen isotopes, so we focus here on $\delta^{13}C_{POC}$ and $\delta^{30}Si_{BSi}$. Since our record does not extend beyond December 2018, and we do not capture the first 3 weeks of January 2018 when fluxes are likely high, we do not record the initial value at this time, however, we would expect $\delta^{13}C_{POC}$ to be even more negative at this time. We we cannot determine if $\delta^{13}C_{POC}$ and $\delta^{30}Si_{BSi}$ would return to values akin to that in period 1 in the following late spring-summer season (January 2019). We saw a shift in the baseline $\delta^{13}C_{POC}$ from a mean of -28.31 ‰ in January 2018 at the time of our first measurements in January 2018 at the start of period 1, to -25.88 ‰ in September at the start of period 2. This coincided with a change in community structure, with abundance dominated by *Fragilariopsis spp.* in period 1 to a more mixed community in period 2. Of the abundant phytoplankton species (>5%, Figure 4A, BC), we find statistically significant linear relationships between $\delta^{13}C_{POC}$ and percent abundance for *Fragilariopsis spp.* (empty: R^2 = 0.926, p<0.001), *Thalassionema nitzschioides* (live: R^2 = 0.774, p=0.004;, empty: R^2 = 0.844, p=0.001), and *Chaetoceros spp. (resting spore)* (R^2 = 0.732, p=0.007). We stress this is based on only 8 samples. Nevertheless, these robust samples show that there was a shift in phytoplankton community structure. TThough *Fragilariopsis spp.* were mainly empty cells, colonisation by bacteria (Grossart et al., 2003; Kiørboe et al., 2003) may facilitate carbon transfer within and on these cells, and certainly the live cells of *T. nitzschioides* and resting spores of *Chaetoceros spp.* would act as agents of carbon transfer (Agusti et al., 2015; Salter et al., 2012; Rembauville et al., 2016).

We examine whether this shift in phytoplankton community composition is associated with a change in SA:V (Table 2) since greater fractionation of carbon in smaller phytoplankton cells with higher SA:V is well observed in the literature (e.g. Popp et al., 1998; Tuerena et al., 2019). There was a statistically significant (paired t-test, p=0.008) difference in the community SA:V between productive periods, increasing from 0.35 μm^2 μm^{-3} in period 1 to 0.51 μm^2 μm^{-3} in period 2. However, this would result in increased isotopic fractionationact in opposition to the decreased baseline fractionation at the start of period 2 compared to period 1 during period 2, in opposition to what we observed. We note here, that as only intact cells were counted, the measured SA:V ratios may not fully account forrepresent the isotopic composition of the trap material due to the presence of fragmented material. It is possible that there was a change in the mechanismthod of carbon uptake with the more mixed phytoplankton community in period 2 using HCO_3^- instead of CO_2 or employing carbon concentrating mechanisms (CCMs), both of which would result in higher $\delta^{13}C_{POC}$ than the diffusive uptake of CO_2 via Rubisco (Raven, 1997; Cassar et al., 2004). Studies show that there is much diversity amongst diatoms in the use of CCMs and many are able to take up both CO_2 and HCO_3^- (Trimborn et al., 2009; Roberts et al., 2007; Shen et al., 2017; Young et al., 2016). We suggest that species driven differences in carbon uptake mechanisms account in part for the differing baselines in $\delta^{13}C_{POC}$ that we observed at the start of period 1 and period 2during the two main productive periods.

Table 2: Phytoplankton cell community surface area to volume (SA:V) ratios measured in deep and shallow sediment traps for samples enumerated in both productive periods 1 and 2.

Bottle open date	Depth	Period	Mean community SA:V
25/01/2018	Shallow	1	0.39
01/02/2018	Shallow	1	0.35
01/02/2018	Deep	1	0.33

15/02/2018	Deep	1	0.32
01/12/2018	Deep	2	0.53
01/12/2018	Shallow	2	0.48
15/12/2018	Deep	2	0.53
15/12/2018	Shallow	2	0.52

721

722 WThe fact that we also observed a shifting baselineshift in the mean flux-weighted $\delta^{30}Si_{BSi}$ ratios
723 (Table 1) between period 1 and period 2. , and that, with With the exception of one culture study
724 (Sutton et al., 2013), systematic species driven shifts in $\delta^{30}Si_{BSi}$ fractionation have not been observed
725 (e.g., De La Rocha et al., 1997), suggestings that there may be an additional driver of the changing
726 isotopic baselines ratioswe observed between the start of period 1 and period 2. Since, prior to our
727 first measurements there had been a long-lasting phytoplankton bloom (Figure S2), we would expect
728 production to have utilised much of the light ^{28}Si, resulting in particles with enriched $\delta^{30}Si_{BSi}$ reaching
729 the trap in January 2018. However, we observe isotopically light mean values of +0.48 ‰ at the start
730 of sampling at the end of Januaryperiod 1, suggesting that there must have been a resupply of ^{28}Si.
731 Physical mixing, bringing deep and benthic waters rich in nutrients, including iron, to the surface
732 waters around South Georgia, are known to support the large blooms occurring downstream of
733 South Georgia (Matano et al., 2020; Nielsdóttir et al., 2012) and could supply both ^{12}C-enriched
734 dissolved inorganic carbon and ^{28}Si-enriched silicic acid. Additional nutrients could also be supplied
735 to our study region by glacial discharge associated with isotopically light silicon isotopic signatures
736 (Matano et al., 2020; Hatton et al., 2019), or benthic fluxes from shelf sediments, likely also releasing
737 isotopically light DSi (Ng et al., 2020; Cassarino et al., 2020; Closset et al., 2022). Therefore, we
738 suggest that low values (increased fractionation) of $\delta^{13}C_{POC}$ and $\delta^{30}Si_{BSi}$, during period 1, relate to
739 increased nutrient availability enabling full expression of the isotopic fractionation and thus
740 isotopically light particulate material to reach the sediment trap.

741 The ocean circulation in our study region is complex and variable on fine spatial and temporal scales,
742 affecting horizontal and vertical velocities (e.g. Boehme et al., 2008). It is clear from the currents
743 measured at the depths of our two traps (Figure S1), that both the direction and magnitude of the
744 flow can vary within and between seasonsally and is not necessarily consistent between the two
745 depths. There are thus potentially different source regions for material in the two traps at certain
746 times of the year. We lack the full depth resolution of vertical and horizontal velocity fields and
747 information on sinking rates to confirm this, but previous studies have highlighted variability in the
748 locations of the Southern Antarctic Circumpolar Current Front and the Polar Front, as well as eddies
749 generated from these fronts, in our study region (Moore et al., 1999; Boehme et al., 2008;
750 Whitehouse et al., 1996). We suggest that variability in ocean current velocities could drive explain
751 different isotopic ratiosbaselines in period 1 and 2, through the supply of material to the traps from
752 a different source region with differing nutrient and remineralisation regimes. Different source
753 watersThis would impact nutrient availability including iron supply, uptake and recycling (Hawco et
754 al., 2021; Ellwood et al., 2020), which in turn influences species composition, nutrient utilisation and
755 uptake rates (e.g. Meyerink et al., 2019). This highlights the importance of making synchronous, and
756 full depth resolution measurements of, physical processes such as current strength and direction, to
757 be able to distinguish between spatial and temporal drivers of shifts in species composition, particle
758 flux and isotopic composition.

759 Since trophic transfer is known to impact both carbon and nitrogen isotope compositions of organic

760 matter, the presence of moults and faecal pellets in trap samples are also important to consider. An

761 incubation study focussed on *Euphausia superba* found that the $\delta^{15}N$ of the *E. superba* faecal pellets

762 was always lower than that of the copepods they ingested, though still higher than that of POM

763 (Schmidt et al., 2003)~~., and~~ Additionally, Tamelander et al. (2006) measured faecal pellets produced

764 by copepods with depleted ^{15}N compared to the algal food source. Though a few studies on

765 temperate and subtropical copepods showed that the faecal material had similar or slightly higher

766 $\delta^{15}N$ than the food source (Altabet and Small, 1990; Checkley and Entzeroth, 1985), there is not a

767 consistent fractionation effect of egestion, for either $\delta^{15}N$ or $\delta^{13}C$, which may relate to compositional

768 differences (protein, carbohydrate, lipid) and their isotopic values (Tamelander et al., 2006). We are

769 therefore not able to determine the impact of faecal pellets or moults on the isotopic composition of

770 our samples. As phytoplankton material dominated at the times of peak flux, we suggest that the

771 importance of faecal pellets and moults may be greater during periods of lower flux, however we

772 cannot rule out their contribution during the bloom periods. We suggest that it would be highly

773 informative to conduct particle specific isotope analysis of common particle types in sediment traps

774 such as faecal pellets, phytoplankton detritus and zooplankton moults, to improve our ability to

775 determine the impact of particle flux composition on bulk isotope compositions.

776

777 ~~Summary~~Conclusion

778 ~~We observed that the fluxes and isotopic ratios of sinking particulate material well represent the~~ The

779 seasonal cycles in primary productivity and nutrient uptake in surface waters at our study site in the

780 Scotia Sea are reflected in the fluxes and isotopic ratios of sinking particulate material. We find that~~,~~

781 ~~at our study site,~~ most remineralisation occurs in the upper 400 m of the water column~~,~~ and below

782 this the magnitude of the flux of sinking material is relatively consistent, supported by consistency in

783 POC:PON ratios. ~~material is altered relatively little. This suggests that particles reaching 400 m likely~~

784 ~~facilitate the transfer of carbon much deeper in the ocean, sequestering carbon for longer time~~

785 ~~periods.~~ We find that particulate fluxes of C,~~N~~ and BSi~~ ~~ are t~~ightly~~~~ypically~~ coupled which highlights

786 the importance of siliceous material in the transfer of POC to depth. We suggest that a change in

787 phytoplankton community structure can at least part explain the shifts in carbon isotopic

788 composition between the two productive periods measured here. ~~, and that the degree to which~~

789 ~~trends in bulk isotopic compositions are coupled provides information on nutrient and~~

790 ~~remineralisation regimes, and associated shifts in phytoplankton community structure.~~ Though

791 complex, seasonal patterns in isotopic composition of particulate material reaching the sediment

792 traps do reflect the degree and type of nutrient utilisation in the source waters. ~~We suggest that it~~

793 ~~would be highly informative to conduct particle specific isotope analysis of common particle types in~~

794 ~~sediment traps such as faecal pellets, phytoplankton detritus and zooplankton moults, to improve~~

795 ~~our ability to determine the impact of particle flux composition on bulk isotope compositions.~~ Our

796 data also ~~reveals the~~suggests an importance of ~~the~~ laterally suppli~~ed~~y ~~of~~material to the sediment

797 traps and s~~upport~~uggests seasonal differences in source regions. ~~This highlights the importance of~~

798 ~~making synchronous, and full depth resolution measurements of, physical processes such as current~~

799 ~~strength and direction, to be able to distinguish between spatial and temporal drivers of shifts in~~

800 ~~species composition, particle flux and isotopic composition.~~ Our results highlight how, t~~T~~hrough

801 more detailed mechanistic understanding of the drivers of POC flux, and biogeochemical cycling, we

can improve estimates of the current and future strength of the biological carbon pump BCP and the
ocean's role as a CO_2 sink.

Data availability

Author contributions

AB and CM conceived the study and participated in fieldwork to collect samples. AB conducted
laboratory analysis with support from TW, LF, and UD for isotope analysis. MW conducted
phytoplankton analysis and provided intellectual input on phytoplankton community composition.
SH and KH provided support for isotopic analysis and contributed to the interpretation of the data
and implications. CC supported uncertainty analysis. All authors contributed text to the manuscript.

Competing Interests

The authors declare that they have no conflict of interest.

Acknowledgements

References

Agusti, S., González-Gordillo, J. I., Vaqué, D., Estrada, M., Cerezo, M. I., Salazar, G., Gasol, J. M., and
Duarte, C. M.: Ubiquitous healthy diatoms in the deep sea confirm deep carbon injection by the
biological pump, Nat. Commun., 6, 1–8, https://doi.org/10.1038/ncomms8608, 2015.

Altabet, M. A. and Small, L. F.: Nitrogen isotopic ratios in fecal pellets produced by marine
Zooplankton, Geochim. Cosmochim. Acta, 54, 155–163, https://doi.org/10.1016/0016-
7037(90)90203-W, 1990.

Altabet, M. A., Deuser, W. G., Honjo, S., and Stienen, C.: Seasonal and depth-related changes in the

839   source of sinking particles in the North Atlantic, Nature, 354, 136–139,
840   https://doi.org/10.1038/354136a0, 1991.

841   Annett, A. L., Henley, S. F., Venables, H. J., Meredith, M. P., Clarke, A., and Ganeshram, R. S.: Silica
842   cycling and isotopic composition in northern Marguerite Bay on the rapidly-warming western
843   Antarctic Peninsula, Deep. Res. Part II Top. Stud. Oceanogr., 139, 132–142,
844   https://doi.org/10.1016/j.dsr2.2016.09.006, 2017.

845   Armstrong, R. A., Lee, C., Hedges, J. I., Honjo, S., and Wakeham, S. G.: A new, mechanistic model for
846   organic carbon fluxes in the ocean based on the quantitative association of POC with ballast
847   minerals, Deep. Res. Part II Top. Stud. Oceanogr., 49, 219–236, https://doi.org/10.1016/S0967-
848   0645(01)00101-1, 2001.

849   Baumann, M., Joy Paul, A., Taucher, J., Thomas Bach, L., Goldenberg, S., Stange, P., Minutolo, F.,
850   Riebesell, U., and Baumann mbaumann, M.: Drivers of Particle Sinking Velocities in the Peruvian
851   Upwelling System, EGU sphere. Prepr., 2022.

852   Belcher, A., Manno, C., Ward, P., Henson, S. A., Sanders, R., and Tarling, G. A.: Copepod faecal pellet
853   transfer through the meso- and bathypelagic layers in the Southern Ocean in spring, Biogeosciences,
854   14, https://doi.org/10.5194/bg-14-1511-2017, 2017.

855   Belcher, A., Manno, C., Thorpe, S., and Tarling, G.: Acantharian cysts: high flux occurrence in the
856   bathypelagic zone of the Scotia Sea, Southern Ocean, Mar. Biol., 165,
857   https://doi.org/10.1007/s00227-018-3376-1, 2018.

858   Bidigare, R., Hanson, L., Buesseler, K. O., Wakeham, G., Freeman, H., Pancost, R. D., Millero, J.,
859   Steinberg, P., Popp, N., Latasa, M., Landry, R., and Laws, A.: Iron-stimulated changes in 13C
860   fractionation and export by equatorial Pacific phytoplankton: Toward a paleogrowth rate proxy,
861   Paleoceanography, 14, 589–595, https://doi.org/10.1029/1999PA900026, 1999.

862   Boehme, L., Meredith, M. P., Thorpe, S. E., Biuw, M., and Fedak, M.: Antarctic circumpolar current
863   frontal system in the South Atlantic: Monitoring using merged Argo and animal-borne sensor data, J.
864   Geophys. Res., 113, C09012, https://doi.org/10.1029/2007JC004647, 2008.

865   Buesseler, K. O., Antia, A. N., Chen, M., Fowler, S. W., Gardner, W. D., Gustafsson, O., Harada, K.,
866   Michaels, A. F., Rutgers van der Loeff, M., Sarin, M., Steinberg, D. K., and Trull, T.: An assessment of
867   the use of sediment traps for estimating upper ocean particle fluxes, J. Mar. Res., 65, 345–416,
868   https://doi.org/10.1357/002224007781567621, 2007.

869   Cassar, N., Laws, E. A., Bidigare, R. R., and Popp, B. N.: Bicarbonate uptake by Southern Ocean
870   phytoplankton, Global Biogeochem. Cycles, 18, 1–10, https://doi.org/10.1029/2003GB002116, 2004.

871   Cassarino, L., Hendry, K. R., Meredith, M. P., Venables, H. J., and De La Rocha, C. L.: Silicon isotope
872   and silicic acid uptake in surface waters of Marguerite Bay, West Antarctic Peninsula, Deep. Res. Part
873   II Top. Stud. Oceanogr., 139, 143–150, https://doi.org/10.1016/j.dsr2.2016.11.002, 2017.

874   Cassarino, L., Hendry, K., Henley, S. F., Macdonald, E., Arndt, S., Freitas, F. S., Pike, J., and Firing, Y. L.:
875   Sedimentary Nutrient Supply in Productive Hot Spots off the West Antarctic Peninsula Revealed by
876   Silicon Isotopes, Global Biogeochem. Cycles, https://doi.org/10.1029/2019GB006486, 2020.

877   Checkley, D. M. and Entzeroth, L. C.: Elemental and isotopic fractionation of carbon and nitrogen by
878   marine, planktonic copepods and implications to the marine nitrogen cycle, J. Plankton Res., 7, 553–
879   568, https://doi.org/https://doi.org/10.1093/plankt/7.4.553, 1985.

880   Closset, I., Cardinal, D., Bray, S. G., Thil, F., Djouraev, I., Rigual-Hernández, A. S., and Trull, T. W.:
881   Seasonal variations, origin, and fate of settling diatoms in the Southern Ocean tracked by silicon
882   isotope records in deep sediment traps, Global Biogeochem. Cycles, 29, 1495–1510,

883 https://doi.org/10.1002/2015GB005180, 2015.

884 Closset, I., Brzezinski, M. A., Cardinal, D., Dapoigny, A., Jones, J. L., and Robinson, R.: A silicon
885 isotopic perspective on the contribution of diagenesis to the sedimentary silicon budget in the
886 Southern Ocean, Geochim. Cosmochim. Acta, 327, 298–313, 2022.

887 Demarest, M. S., Brzezinski, M. A., and Beucher, C. P.: Fractionation of silicon isotopes during
888 biogenic silica dissolution, Geochim. Cosmochim. Acta, 73, 5572–5583,
889 https://doi.org/10.1016/j.gca.2009.06.019, 2009.

890 DeVries, T.: Atmospheric CO2 and Sea Surface Temperature Variability Cannot Explain Recent
891 Decadal Variability of the Ocean CO2 Sink, Geophys. Res. Lett., 49, 1–17,
892 https://doi.org/10.1029/2021GL096018, 2022.

893 Egan, K. E., Rickaby, R. E. M., Leng, M. J., Hendry, K. R., Hermoso, M., Sloane, H. J., Bostock, H., and
894 Halliday, A. N.: Diatom silicon isotopes as a proxy for silicic acid utilisation: A Southern Ocean core
895 top calibration, Geochim. Cosmochim. Acta, 96, 174–192,
896 https://doi.org/10.1016/j.gca.2012.08.002, 2012.

897 Ellwood, M. J., Strzepek, R. F., Strutton, P. G., Trull, T. W., Fourquez, M., and Boyd, P. W.: Distinct
898 iron cycling in a Southern Ocean eddy, Nat. Commun., 11, 1–8, https://doi.org/10.1038/s41467-020-
899 14464-0, 2020.

900 Fischer, G., Gersonde, R., and Wefer, G.: Organic carbon, biogenic silica and diatom fluxes in the
901 marginal winter sea-ice zone and in the Polar Front Region: Interannual variations and differences in
902 composition, Deep. Res. Part II Top. Stud. Oceanogr., 49, 1721–1745,
903 https://doi.org/10.1016/S0967-0645(02)00009-7, 2002.

904 Friedrich, J. and Rutgers van der Loeff, M. M.: A two-tracer (210Po-234Th) approach to distinguish
905 organic carbon and biogenic silica export flux in the Antarctic Circumpolar Current, Deep. Res. Part I
906 Oceanogr. Res. Pap., 49, 101–120, https://doi.org/10.1016/S0967-0637(01)00045-0, 2002.

907 Georg, R. B., Reynolds, B. C., Frank, M., and Halliday, A. N.: New sample preparation techniques for
908 the determination of Si isotopic compositions using MC-ICPMS, Chem. Geol., 235, 95–104,
909 https://doi.org/10.1016/j.chemgeo.2006.06.006, 2006.

910 Giering, S. L. C., Cavan, E. L., Basedow, S. L., Briggs, N., Burd, A. B., Darroch, L. J., Guidi, L., Irisson, J.
911 O., Iversen, M. H., Kiko, R., Lindsay, D., Marcolin, C. R., McDonnell, A. M. P., Möller, K. O., Passow, U.,
912 Thomalla, S., Trull, T. W., and Waite, A. M.: Sinking Organic Particles in the Ocean—Flux Estimates
913 From in situ Optical Devices, Front. Mar. Sci., 6, https://doi.org/10.3389/fmars.2019.00834, 2020.

914 Gleiber, M. R., Steinberg, D. K., and Ducklow, H. W.: Time series of vertical flux of zooplankton fecal
915 pellets on the continental shelf of the western Antarctic Peninsula, Mar. Ecol. Prog. Ser., 471, 23–36,
916 https://doi.org/10.3354/meps10021, 2012.

917 Glibert, P. M., Wilkerson, F. P., Dugdale, R. C., Raven, J. A., Dupont, C. L., Leavitt, P. R., Parker, A. E.,
918 Burkholder, J. M., and Kana, T. M.: Pluses and minuses of ammonium and nitrate uptake and
919 assimilation by phytoplankton and implications for productivity and community composition, with
920 emphasis on nitrogen-enriched conditions, Limnol. Oceanogr., 61, 165–197,
921 https://doi.org/10.1002/lno.10203, 2016.

922 González, H. E., Daneri, G., Iriarte, J. L., Yannicelli, B., Menschel, E., Barría, C., Pantoja, S., and
923 Lizárraga, L.: Carbon fluxes within the epipelagic zone of the Humboldt Current System off Chile: The
924 significance of euphausiids and diatoms as key functional groups for the biological pump, Prog.
925 Oceanogr., 83, 217–227, https://doi.org/10.1016/j.pocean.2009.07.036, 2009.

926 Grasse, P., Brzezinski, M. A., Cardinal, D., De Souza, G. F., Andersson, P., Closset, I., Cao, Z., Dai, M.,

927 Ehlert, C., Estrade, N., François, R., Frank, M., Jiang, G., Jones, J. L., Kooijman, E., Liu, Q., Lu, D.,
928 Pahnke, K., Ponzevera, E., Schmitt, M., Sun, X., Sutton, J. N., Thil, F., Weis, D., Wetzel, F., Zhang, A.,
929 Zhang, J., and Zhang, Z.: GEOTRACES inter-calibration of the stable silicon isotope composition of
930 dissolved silicic acid in seawater, J. Anal. At. Spectrom., 32, 562–578,
931 https://doi.org/10.1039/c6ja00302h, 2017.

932 Grasse, P., Haynert, K., Doering, K., Geilert, S., Jones, J. L., Brzezinski, M. A., and Frank, M.: Controls
933 on the Silicon Isotope Composition of Diatoms in the Peruvian Upwelling, Front. Mar. Sci., 8, 1–15,
934 https://doi.org/10.3389/fmars.2021.697400, 2021.

935 Grossart, H. P., Kiørboe, T., Tang, K., and Ploug, H.: Bacterial colonization of particles: Growth and
936 interactions, Appl. Environ. Microbiol., 69, 3500–3509, https://doi.org/10.1128/AEM.69.6.3500-
937 3509.2003, 2003.

938 Hansman, R. L. and Sessions, A. L.: Measuring the in situ carbon isotopic composition of distinct
939 marine plankton populations sorted by flow cytometry, Limnol. Oceanogr. Methods, 14, 87–99,
940 https://doi.org/10.1002/lom3.10073, 2016.

941 Hasle, G. R. and Syvertsen, E. E.: Chapter 2 – Marine Diatoms, in: Identifying Marine Phytoplankton,
942 edited by: Tomas, C. R., Academic Press, San Diego, 5–385, 1997.

943 Hatton, J. E., Hendry, K. R., Hawkings, J. R., Wadham, J. L., Opfergelt, S., Kohler, T. J., Yde, J. C., Stibal,
944 M., and Žárský, J. D.: Silicon isotopes in Arctic and sub-Arctic glacial meltwaters: The role of
945 subglacial weathering in the silicon cycle, Proc. R. Soc. A Math. Phys. Eng. Sci., 475,
946 https://doi.org/10.1098/rspa.2019.0098, 2019.

947 Hawco, N. J., Barone, B., Church, M. J., Babcock-Adams, L., Repeta, D. J., Wear, E. K., Foreman, R. K.,
948 Björkman, K. M., Bent, S., Van Mooy, B. A. S., Sheyn, U., DeLong, E. F., Acker, M., Kelly, R. L., Nelson,
949 A., Ranieri, J., Clemente, T. M., Karl, D. M., and John, S. G.: Iron Depletion in the Deep Chlorophyll
950 Maximum: Mesoscale Eddies as Natural Iron Fertilization Experiments, Global Biogeochem. Cycles,
951 35, 1–18, https://doi.org/10.1029/2021GB007112, 2021.

952 Hendry, K. R. and Brzezinski, M. A.: Using silicon isotopes to understand the role of the Southern
953 Ocean in modern and ancient biogeochemistry and climate, Quat. Sci. Rev., 89, 13–26,
954 https://doi.org/10.1016/j.quascirev.2014.01.019, 2014.

955 Hendry, K. R. and Robinson, L. F.: The relationship between silicon isotope fractionation in sponges
956 and silicic acid concentration: Modern and core-top studies of biogenic opal, Geochim. Cosmochim.
957 Acta, 81, 1–12, https://doi.org/10.1016/j.gca.2011.12.010, 2012.

958 Henley, S. F., Annett, A. L., Ganeshram, R. S., Carson, D. S., Weston, K., Crosta, X., Tait, A., Dougans,
959 J., Fallick, A. E., and Clarke, A.: Factors influencing the stable carbon isotopic composition of
960 suspended and sinking organic matter in the coastal Antarctic sea ice environment, Biogeosciences,
961 9, 1137–1157, https://doi.org/10.5194/bg-9-1137-2012, 2012.

962 Hillebrand, H., Dürselen, C. D., Kirschtel, D., Pollingher, U., and Zohary, T.: Biovolume calculation for
963 pelagic and benthic microalgae, J. Phycol., 35, 403–424, https://doi.org/10.1046/j.1529-
964 8817.1999.3520403.x, 1999.

965 Honjo, S., Francois, R., Manganini, S., Dymond, J., and Collier, R.: Particle fluxes to the interior of the
966 Southern Ocean in the Western Pacific sector along 170°W, Deep. Res. Part II, 47, 3521–3548,
967 https://doi.org/10.1016/S0967-0645(00)00077-1, 2000.

968 Iversen, M. H., Pakhomov, E. A., Hunt, B. P. V, Jagt, H. Van Der, Wolf-gladrow, D., and Klaas, C.:
969 Sinkers or floaters? Contribution from salp pellets to the export flux during a large bloom event in
970 the Southern Ocean, Deep Sea Res. Part II Top. Stud. Oceanogr., 138, 116–125,

971   https://doi.org/10.1016/j.dsr2.2016.12.004, 2017.

972   Kiørboe, T., Tang, K., Grossart, H. P., and Ploug, H.: Dynamics of microbial communities on marine
973   snow aggregates: Colonization, growth, detachment, and grazing mortality of attached bacteria,
974   Appl. Environ. Microbiol., 69, 3036–3047, https://doi.org/10.1128/AEM.69.6.3036-3047.2003, 2003.

975   Korb, R. E., Whitehouse, M. J., Atkinson, A., and Thorpe, S.: Magnitude and maintenance of the
976   phytoplankton bloom at South Georgia: a naturally iron-replete environment, Mar. Ecol. Prog. Ser.,
977   368, 75–91, https://doi.org/10.3354/meps07525, 2008.

978   Korb, R. E., Whitehouse, M. J., Ward, P., Gordon, M., Venables, H. J., and Poulton, A. J.: Regional and
979   seasonal differences in microplankton biomass, productivity, and structure across the Scotia Sea:
980   Implications for the export of biogenic carbon, Deep Sea Res. Part II Top. Stud. Oceanogr., 59–60,
981   67–77, https://doi.org/10.1016/j.dsr2.2011.06.006, 2012.

982   Kwon, E., Primeau, F., and Sarmiento, J.: The impact of remineralization depth on the air-sea carbon
983   balance, Nat. Geosci., 2, 630–635, 2009.

984   De La Rocha, C. L., Brzezinski, M. A., and DeNiro, M. J.: Fractionation of silicon isotopes by marine
985   diatoms during biogenic silica formation, Geochim. Cosmochim. Acta, 61, 5051–5056,
986   https://doi.org/10.1016/S0016-7037(97)00300-1, 1997.

987   Manno, C., Stowasser, G., Enderlein, P., Fielding, S., and Tarling, G. A.: The contribution of
988   zooplankton faecal pellets to deep-carbon transport in the Scotia Sea (Southern Ocean),
989   Biogeosciences, 12, 1955–1965, https://doi.org/10.5194/bg-12-1955-2015, 2015.

990   Manno, C., Fielding, S., Stowasser, G., Murphy, E. J., and Thorpe, S. E.: Continuous moulting by
991   Antarctic krill drives major, Nat. Commun., 16, 6051, https://doi.org/10.1038/s41467-020-19956-7,
992   2020.

993   Matano, R. P., Combes, V., Young, E. F., and Meredith, M. P.: Modeling the Impact of Ocean
994   Circulation on Chlorophyll Blooms Around South Georgia, Southern Ocean, J. Geophys. Res. Ocean.,
995   125, 1–18, https://doi.org/10.1029/2020JC016391, 2020.

996   Medlin, L. K. and Priddle, J.: Polar marine diatoms, British Antarctic Survey, Cambridge, UK, 214 pp.,
997   1990.

998   Meyerink, S. W., Boyd, P. W., Maher, W. A., Milne, A., Strzepek, R., and Ellwood, M. J.: Putting the
999   silicon cycle in a bag: Field and mesocosm observations of silicon isotope fractionation in subtropical
1000 waters east of New Zealand, Mar. Chem., 213, 1–12,
1001 https://doi.org/10.1016/j.marchem.2019.04.008, 2019.

1002 Michener, R. and Lajtha, K.: Stable Isotopes in Ecology and Environmental Science: Second Edition,
1003 1–566 pp., https://doi.org/10.1002/9780470691854, 2008.

1004 Minagawa, M. and Wada, E.: Stepwise enrichment of 15N along food chains: Further evidence and
1005 the relation between δ15N and animal age, Geochim. Cosmochim. Acta, 48, 1135–1140,
1006 https://doi.org/10.1016/0016-7037(84)90204-7, 1984.

1007 Mincks, S. L., Smith, C. R., Jeffreys, R. M., and Sumida, P. Y. G.: Trophic structure on the West
1008 Antarctic Peninsula shelf: Detritivory and benthic inertia revealed by δ13C and δ15N analysis, Deep.
1009 Res. Part II Top. Stud. Oceanogr., 55, 2502–2514, https://doi.org/10.1016/j.dsr2.2008.06.009, 2008.

1010 Montoya, J. P.: Natural abundance of 15N in marine planktonic ecosystems, in: Stable Isotopes in
1011 Ecology and Environmental Science: Second Edition, edited by: Michener, R. and Lajtha, K., Blackwell
1012 Publishing, 1–566, https://doi.org/10.1002/9780470691854, 2007.

1013 Moore, J. K., Abbott, M. R., and Richman, J. G.: Location and dynamics of the Antarctic Polar Front

1014 from satellite sea surface temperature data, J. Geophys. Res. Ocean., 104, 3059–3073,
1015 https://doi.org/10.1029/1998JC900032, 1999.

1016 Ng, H. C., Cassarino, L., Pickering, R. A., Woodward, E. M. S., Hammond, S. J., and Hendry, K. R.:
1017 Sediment efflux of silicon on the Greenland margin and implications for the marine silicon cycle,
1018 Earth Planet. Sci. Lett., 529, 115877, https://doi.org/10.1016/j.epsl.2019.115877, 2020.

1019 Nielsdóttir, M. C., Bibby, T. S., Moore, C. M., Hinz, D. J., Sanders, R., Whitehouse, M., Korb, R., and
1020 Achterberg, E. P.: Seasonal and spatial dynamics of iron availability in the Scotia Sea, Mar. Chem.,
1021 130–131, 62–72, https://doi.org/10.1016/j.marchem.2011.12.004, 2012.

1022 Opfergelt, S. and Delmelle, P.: Silicon isotopes and continental weathering processes: Assessing
1023 controls on Si transfer to the ocean, Comptes Rendus - Geosci., 344, 723–738,
1024 https://doi.org/10.1016/j.crte.2012.09.006, 2012.

1025 Orsi, H., Whitworth III, T., and Nowlin Jr, W. D.: On the meridional extent and fronts of the Antarctic
1026 Circumpolar Current, Deep Sea Res. Part I Oceanogr. Res. Pap., 42, 641–673,
1027 https://doi.org/10.1016/0967-0637(95)00021-W, 1995.

1028 Passow, U. and De La Rocha, C. L.: Accumulation of mineral ballast on organic aggregates, Global
1029 Biogeochem. Cycles, 20, 1–7, https://doi.org/10.1029/2005GB002579, 2006.

1030 Pauli, N.-C., Flintrop, C. M., Konrad, C., Pakhomov, E. A., Swoboda, S., Koch, F., Wang, X.-L., Zhang, J.-
1031 C., Brierley, A. S., Bernasconi, M., Meyer, B., and Iversen, M. H.: Krill and salp faecal pellets
1032 contribute equally to the carbon flux at the Antarctic Peninsula, Nat. Commun., 12, 7168,
1033 https://doi.org/10.1038/s41467-021-27436-9, 2021.

1034 Ploug, H., Iversen, M. H., and Fischer, G.: Ballast, sinking velocity, and apparent diffusivity within
1035 marine snow and zooplankton fecal pellets: Implications for substrate turnover by attached bacteria,
1036 Limnol. Oceanogr., 53, 1878–1886, 2008.

1037 Popp, B. N., Laws, E. A., Bidigare, R. R., Dore, J. E., Hanson, K. L., and Wakeham, S. G.: Effect of
1038 phytoplankton cell geometry on carbon isotopic fractionation, Geochim. Cosmochim. Acta, 62, 69–
1039 77, https://doi.org/10.1016/S0016-7037(97)00333-5, 1998.

1040 Popp, B. N., Trull, T., Kenig, F., Wakeham, S. G., Rust, T. M., Tilbrook, B., Griffiths, F. B., Wright, S. W.,
1041 Marchant, H. J., Bidigare, R. R., and Laws, E. A.: Controls on the carbon isotopic composition of
1042 Southern Ocean phytoplankton, Global Biogeochem. Cycles, 13, 827–843,
1043 https://doi.org/10.1029/1999GB900041, 1999.

1044 Priddle, J. and Fryxell, G.: Handbook of the common plankton diatoms of the Southern Ocean:
1045 Centrales except the genus Thalassiosira, British Antarctic Survey, Cambridge, UK, 159 pp., 1985.

1046 Rau, G. H., Froelich, P. N., Takahashi, T., and J., D. M. D.: Does sedimentary organic $\delta^{13}C$ record
1047 variations in quaternary ocean [CO2(aq)], Paleoceanography, 6, 335–347, 1991.

1048 Raven, J. A.: Inorganic Carbon Acquisition by Marine Autotrophs, Adv. Bot. Res., 27, 85–209,
1049 https://doi.org/10.1016/S0065-2296(08)60281-5, 1997.

1050 Rembauville, M., Blain, S., Armand, L., Quéguiner, B., and Salter, I.: Export fluxes in a naturally iron-
1051 fertilized area of the Southern Ocean – Part 2: Importance of diatom resting spores and faecal
1052 pellets for export, Biogeosciences, 12, 3171–3195, https://doi.org/10.5194/bg-12-3171-2015, 2015.

1053 Rembauville, M., Manno, C., Tarling, G. A., Blain, S., and Salter, I.: Strong contribution of diatom
1054 resting spores to deep-sea carbon transfer in naturally iron-fertilized waters downstream of South
1055 Georgia, Deep. Res. Part I, 115, 22–35, https://doi.org/10.1016/j.dsr.2016.05.002, 2016.

1056 Reynolds, B. C., Aggarwal, J., André, L., Baxter, D., Beucher, C., Brzezinski, M. A., Engström, E., Georg,

1057 R. B., Land, M., Leng, M. J., Opfergelt, S., Rodushkin, I., Sloane, H. J., Van Den Boorn, S. H. J. M.,
1058 Vroon, P. Z., and Cardinal, D.: An inter-laboratory comparison of Si isotope reference materials, J.
1059 Anal. At. Spectrom., 22, 561–568, https://doi.org/10.1039/b616755a, 2007.

1060 Roberts, K., Granum, E., Leegood, R. C., and Raven, J. A.: Carbon acquisition by diatoms, Photosynth.
1061 Res., 93, 79–88, https://doi.org/10.1007/s11120-007-9172-2, 2007.

1062 Roca-Marti, M., Puigcorbé, V., Iversen, M. H., Rutgers van der Loeff, M., Klaas, C., Cheah, W.,
1063 Bracher, A., and Masqué, P.: High particulate organic carbon export during the decline of a vast
1064 diatom bloom in the Atlantic sector of the Southern Ocean, Deep Sea Res. Part II Top. Stud.
1065 Oceanogr., 138, 102–115, https://doi.org/10.1016/j.dsr2.2015.12.007, 2017.

1066 Salter, I., Kemp, A. E. S. S., Moore, C. M., Lampitt, R. S., Wolff, G. A., and Holtvoeth, J.: Diatom resting
1067 spore ecology drives enhanced carbon export from a naturally iron-fertilized bloom in the Southern
1068 Ocean, Global Biogeochem. Cycles, 26, 1–17, https://doi.org/10.1029/2010GB003977, 2012.

1069 Sathyendranath, S., Brewin, R., Brockmann, C., Brotas, V., Calton, B., Chuprin, A., Cipollini, P., Couto,
1070 A., Dingle, J., Doerffer, R., Donlon, C., Dowell, M., Farman, A., Grant, M., Groom, S., Horseman, A.,
1071 Jackson, T., Krasemann, H., Lavender, S., Martinez-Vicente, V., Mazeran, C., Mélin, F., Moore, T.,
1072 Müller, D., Regner, P., Roy, S., Steele, C., Steinmetz, F., Swinton, J., Taberner, M., Thompson, A.,
1073 Valente, A., Zühlke, M., Brando, V., Feng, H., Feldman, G., Franz, B., Frouin, R., Gould, R., Hooker, S.,
1074 Kahru, M., Kratzer, S., Mitchell, B., Muller-Karger, F., Sosik, H., Voss, K., Werdell, J., and Platt, T.: An
1075 Ocean-Colour Time Series for Use in Climate Studies: The Experience of the Ocean-Colour Climate
1076 Change Initiative (OC-CCI), Sensors, 19, 4285, https://doi.org/10.3390/s19194285, 2019.

1077 Sathyendranath, S., Jackson, T., Brockmann, C., Brotas, V., Calton, B., Chuprin, A., Clements, O.,
1078 Cipollini, P., Danne, O., Dingle, J., Donlon, C., Grant, M., Groom, S., Krasemann, H., Lavender, S.,
1079 Mazeran, C., Mélin, F., Müller, D., Steinmetz, F., Valente, A., Zühlke, M., Feldman, G., Franz, B.,
1080 Frouin, R., Werdell, J., and Platt, T.: ESA Ocean Colour Climate Change Initiative (Ocean_Colour_cci):
1081 Version 5.0 Data, NERC EDS Cent. Environ. Data Anal.,
1082 https://doi.org/10.5285/1dbe7a109c0244aaad713e078fd3059a, 2021.

1083 Schmidt, K., Atkinson, A., Stübing, D., McClelland, J. W., Montoya, J. P., and Voss, M.: Trophic
1084 relationships among Southern Ocean copepods and krill: Some uses and limitations of a stable
1085 isotope approach, Limnol. Oceanogr., 48, 277–289, https://doi.org/10.4319/lo.2003.48.1.0277,
1086 2003.

1087 Scott, F. J. and Marchant, H. J. (Eds.): Antarctic Marine Protists, Australian Biological Resources
1088 Study, Canberra, 2005.

1089 Shen, C., Dupont, C. L., and Hopkinson, B. M.: The diversity of CO2-concentrating mechanisms in
1090 marine diatoms as inferred from their genetic content, J. Exp. Bot., 68, 3937–3948,
1091 https://doi.org/10.1093/jxb/erx163, 2017.

1092 Sigman, D. M. and Fripiat, F.: Nitrogen isotopes in the ocean, Encycl. Ocean Sci., 263–278,
1093 https://doi.org/10.1016/B978-0-12-409548-9.11605-7, 2019.

1094 Smetacek, V., Assmy, P., and Henjes, J.: The role of grazing in structuring Southern Ocean pelagic
1095 ecosystems and biogeochemical cycles, Antarct. Sci., 16, 541–558,
1096 https://doi.org/10.1017/S0954102004002317, 2004.

1097 Strickland, J. and Parsons, T.: A Practical Handbook of Seawater Analysis, Fisheries Research Board of
1098 Canada, 405 pp., https://doi.org/10.2307/1979241, 1972.

1099 Sutton, J. N., Varela, D. E., Brzezinski, M. A., and Beucher, C. P.: Species-dependent silicon isotope
1100 fractionation by marine diatoms, Geochim. Cosmochim. Acta, 104, 300–309,

https://doi.org/10.1016/j.gca.2012.10.057, 2013.

Tamelander, T., Søreide, J. E., Hop, H., and Carroll, M. L.: Fractionation of stable isotopes in the Arctic marine copepod Calanus glacialis: Effects on the isotopic composition of marine particulate organic matter, J. Exp. Mar. Bio. Ecol., 333, 231–240, https://doi.org/10.1016/j.jembe.2006.01.001, 2006.

Thorpe, S. E., Heywood, K. J., Brandon, M. A., and Stevens, D. P.: Variability of the southern Antarctic Circumpolar Current front north of South Georgia, J. Mar. Syst., 37, 87–105, https://doi.org/10.1016/S0924-7963(02)00197-5, 2002.

Torres Valdés, S., Painter, S. C., Martin, A. P., Sanders, R., and Felden, J.: Data compilation of fluxes of sedimenting material from sediment traps in the Atlantic ocean, Earth Syst. Sci. Data, 6, 123–145, https://doi.org/10.5194/essd-6-123-2014, 2014.

Trimborn, S., Wolf-Gladrow, D., Richter, K. U., and Rost, B.: The effect of pCO2 on carbon acquisition and intracellular assimilation in four marine diatoms, J. Exp. Mar. Bio. Ecol., 376, 26–36, https://doi.org/10.1016/j.jembe.2009.05.017, 2009.

Trull, T. W. and Armand, L.: Insights into Southern Ocean carbon export from the δ13c of particles and dissolved inorganic carbon during the SOIREE iron release experiment, Deep. Res. Part II Top. Stud. Oceanogr., 48, 2655–2680, https://doi.org/10.1016/S0967-0645(01)00013-3, 2001.

Tuerena, R. E., Ganeshram, R. S., Humphreys, M. P., Browning, T. J., Bouman, H., and Piotrowski, A. P.: Isotopic fractionation of carbon during uptake by phytoplankton across the South Atlantic subtropical convergence, Biogeosciences, 16, 3621–3635, https://doi.org/10.5194/bg-16-3621-2019, 2019.

Volk, T. and Hoffert, M. I.: Ocean Carbon Pumps: Analysis of relative strengths and efficiencies in ocean driven atmospheric CO_2 changes, in: The carbon cycle and atmospheric CO2:Natural variations Archean to Present, edited by: Sundquist, E. T. and Broecker, W. S., American Geophysical Union, Washington, DC, 99–110, 1985.

Wada, E. and Hattori, A.: Nitrogen isotope effects in the assimilation of inorganic nitrogenous compounds by marine diatoms, Geomicrobiol. J., 1, 85–101, https://doi.org/10.1080/01490457809377725, 1978.

Wada, E., Terazaki, M., Kabaya, Y., and Nemoto, T.: 15N and 13C abundances in the Antartic Ocean with emphasis on the biogeochemical structure of the food web, Deep Sea Res. Part A, Oceanogr. Res. Pap., 34, 829–841, https://doi.org/10.1016/0198-0149(87)90039-2, 1987.

Ward, J. P. J., Hendry, K. R., Arndt, S., Faust, J. C., Freitas, F. S., Henley, S. F., Krause, J. W., März, C., Ng, H. C., Pickering, R. A., and Tessin, A. C.: Stable silicon isotopes uncover a mineralogical control on the benthic silicon cycle in the Arctic Barents Sea, Geochim. Cosmochim. Acta, 329, 206–230, https://doi.org/10.1016/j.gca.2022.05.005, 2022.

Weir, I., Fawcett, S., Smith, S., Walker, D., Bornman, T., and Fietz, S.: Winter biogenic silica and diatom distributions in the Indian sector of the Southern Ocean, Deep. Res. Part I Oceanogr. Res. Pap., 166, 103421, https://doi.org/10.1016/j.dsr.2020.103421, 2020.

Wetzel, F., de Souza, G. F., and Reynolds, B. C.: What controls silicon isotope fractionation during dissolution of diatom opal?, Geochim. Cosmochim. Acta, 131, 128–137, https://doi.org/10.1016/j.gca.2014.01.028, 2014.

White, W. M., Albarède, F., and Télouk, P.: High-precision analysis of Pb isotope ratios by multi-collector ICP-MS, Chem. Geol., 167, 257–270, https://doi.org/10.1016/S0009-2541(99)00182-5, 2000.

1144 Whitehouse, M. J., Priddle, J., Trathan, P. N., and Brandon, M. A.: Substantial open-ocean
1145 phytoplankton blooms to the north of South Georgia, South Atlantic, during summer 1994, Mar.
1146 Ecol. Prog. Ser., 140, 187–197, https://doi.org/10.3354/meps140187, 1996.

1147 Young, J. N., Heureux, A. M. C., Sharwood, R. E., Rickaby, R. E. M., Morel, F. M. M., and Whitney, S.
1148 M.: Large variation in the Rubisco kinetics of diatoms reveals diversity among their carbon-
1149 concentrating mechanisms, J. Exp. Bot., 67, 3445–3456, https://doi.org/10.1093/jxb/erw163, 2016.

1150